

The human brain modulates sniffs according to fine-grained perceptual features of odours

Received: 19 November 2024

Accepted: 22 September 2025

Published online: 12 November 2025

 Check for updates

Vivek Sagar  ^{1,3}✉, Andrew Sheriff¹, Qiaohan Yang  ¹, Naelly Arriaga¹, Guangyu Zhou  ¹, Gregory Lane¹, Thorsten Kahnt  ² & Christina Zelano  ¹✉

Sensorimotor feedback is a fundamental mechanism of active sensing. In olfaction, the primary motor behaviour is the sniff. Thus, in active olfactory sensing, we would expect the dynamics of the sniff to change according to detailed odour characteristics. Furthermore, percept-related modulations of sniffing behaviour should correspond to neural activity in participating brain regions. Here we analysed a high-precision functional MRI dataset including more than 4,300 sniffs per participant taken of 160 odours during ~18 hours of scanning, to probe the relationship between odour-induced sniff modulations and perceptual features at a high level of granularity. We found that fine-grained perceptual odour information—and even odour identity—can be decoded from sniffing dynamics, and that olfactory brain regions, particularly the amygdala, are involved in percept-driven modulation of sniffing behaviour. Thus, olfactory cortical areas participate in real-time modulations of sniffs according to perceptual properties of the odour at a high level of granularity.

Sniffing is the primary motor component of olfaction and the key organizational unit of odour processing^{1–4}. Sniffing behaviour impacts odour percepts^{3,5} and odour responses in the brain^{6–8}, and sniff phase is a key substrate of coding mechanisms in all major olfactory brain regions^{9,10}. Glomeruli in the olfactory bulb are tuned to a particular phase of the sniff⁷, as are mitral and tufted cells that form primary inputs to the piriform cortex^{11,12}. The tight link between sniffing, neural activity and olfactory perception suggests that the olfactory system may contain a sensorimotor feedback loop through which the brain modulates sniffing behaviour in real time according to the odour stimulus. This has been suggested in the literature^{3,13}, and evidence of a coarse version of this mechanism has been established: for example, increased odour concentration and reduced odour pleasantness result in reduced sniff volumes^{13–15}. However, in active sensing, we would expect to see sniffs change according to subtle, detailed nuances of odour perception. Whether this is indeed the case is unknown.

As humans sniff, airflow through the nasal cavity can be precisely measured¹⁶, revealing a rich, temporally evolving signal that is rapidly

modulated by the presence of odour^{3,13}. Interestingly, work conducted in decerebrated perfused brainstem preparations has established that the brainstem is sufficient to evoke sniff modulations in response to the trigeminal components of odours, but the cortex is needed to evoke sniff modulations in response to the purely olfactory perceptual components of odours¹⁷. Thus, if fine-grained perceptual features of odours—used here to refer to the set of perceptual descriptors that can be used to uniquely define an odour’s identity in a multidimensional space—result in predictable sniff modulations, then it follows that there exists an unknown cortical substrate of this effect. Given the rapid interaction between odour and sniff modulations, a cortical candidate for percept-based modulation of sniffs is likely to be a primary olfactory area involved in respiratory control. Intriguingly, the amygdala, which contains primary olfactory cortical areas, has been linked to respiratory control^{18–21} and connects to respiratory nuclei in the brainstem^{22,23}. While studies in patients with epilepsy have established the amygdala’s involvement in respiratory control through a causal role in the generation of apnoea^{18,20,21,24,25}, whether it is involved in olfactory-specific sniff modulations is unknown.

¹Department of Neurology, Feinberg School of Medicine, Northwestern University, Chicago, IL, USA. ²National Institute on Drug Abuse Intramural Research Program, Baltimore, MD, USA. ³Present address: Department of Psychological and Brain Sciences, Dartmouth College, Hanover, NH, USA.

✉e-mail: viveksagar2016@u.northwestern.edu; c-zelano@northwestern.edu

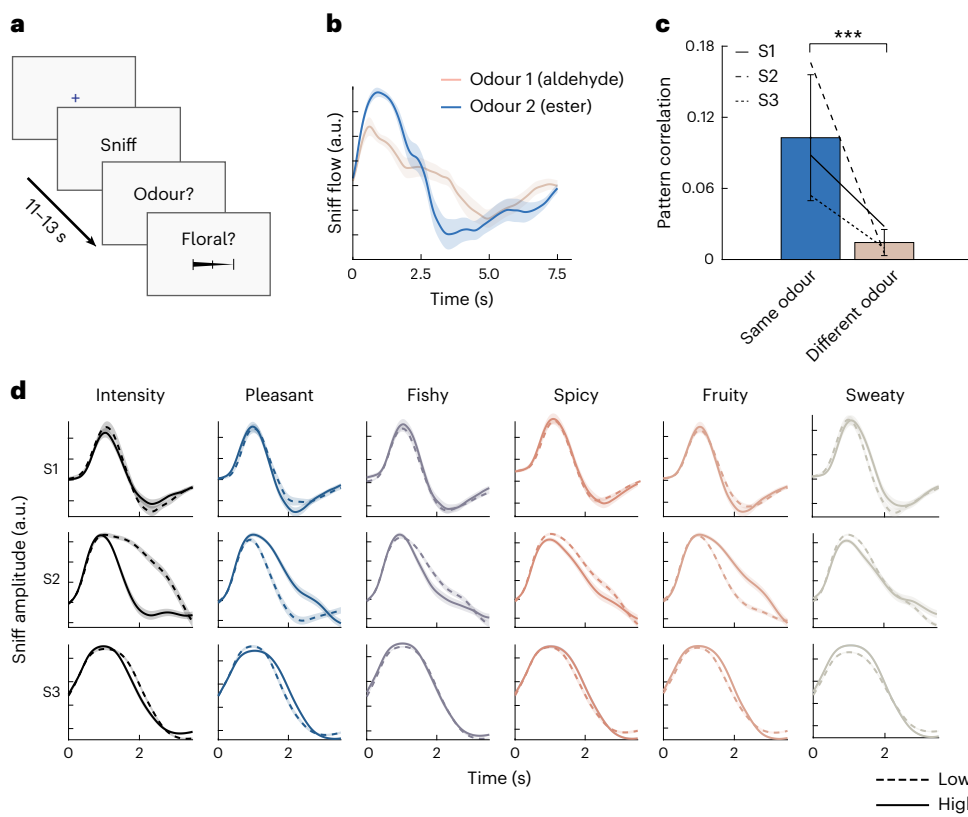


Fig. 1 | Experimental design. **a**, Sniffs were recorded while participants smelled odours during a detection and rating task including 160 odours. **b**, Average sniff trace across 27 trials for 2 odours for S2. Odour 1 is an aldehyde (3-(5-methyl-2-furyl)butanal) with a decayed note. Odour 2 is a fruity ester (ethyl 2-methylpentanoate). Shaded bands indicate the 95% confidence interval (CI). **c**, Pattern correlation analysis showing cross-trial correlation among pairs of trials of the same or of different odours ($r_{\text{same}} = 0.103$; $r_{\text{diff}} = 0.014$; for mean participant,

$P = 0.000$ for each participant; $N = 4,560$ trials in S1 and $N = 4,320$ trials in S2 and S3; two-tailed Wilcoxon rank-sum test). Results were similar after regressing out intensity and pleasantness, as shown in Extended Data Fig. 1c. Data are presented as mean values, and error bars indicate 95% CI. **d**, Example average sniff traces for top and bottom decile trials of perceptual descriptors. Shaded bands indicate 95% CI. *** $P < 0.001$.

Several studies have shown that distributed patterns of neural activity in the olfactory cortex represent odours and their fine-grained perceptual features^{10,26–30}. However, given that these distributed representations change over time³¹, olfactory regions might parse sniffing information for perceptual constancy. This is further evident from recent work showing that ensemble coding in olfactory regions is based on interactions of various neural populations orchestrated by nasal respiration³². Furthermore, olfactory coding is supported by prominent beta and gamma rhythms in the bulb and cortex³³, and sniffing behaviour is known to be a key driver of these temporal dynamics^{34,35}. It is therefore plausible that the olfactory cortex might participate in a perceptual-feature-based sensorimotor feedback loop of sniff modulation, resulting in odour percepts being reflected in the temporal sniff profile, which in turn impacts odour coding. If true, fine-grained olfactory perceptual information should be decodable from sniffing behaviour alone.

Here, we hypothesized that detailed olfactory perceptual information is embedded in sniffing behaviour and that olfactory cortical regions, especially the amygdala, underlie this interaction. To understand how odour information modulates sniffing behaviour, we analysed data from 3 human participants, each smelling 160 odours across more than 4,320 trials inside a magnetic resonance imaging (MRI) scanner (18 h per participant). We found that perceptual odour information including odour identity can be decoded from sniffs, that this decoding occurs at specific phases of the sniff and that olfactory regions, particularly the amygdala, are involved in the percept-based modulation of sniffs. These results suggest that sniff modulations are an integral component underlying odour coding in the brain.

Results

Sniffs are modulated in response to odours

To investigate perceptual modulation of sniffs, we used a previously published dataset³⁶, described in detail in ref. 30, in which 3 human participants smelled 160 odours 27–30 times each, totalling 4,320–4,560 trials during ~18 h of functional (f)MRI scanning per participant. Participants rated the odours on 18 perceptual descriptors, 1 per trial, while their sniffs were recorded (Fig. 1a). Qualitatively, we observed that average sniffs for different odours were distinct. For example in Fig. 1b, odour 1, an aldehyde with a decayed note, is sniffed with a smaller volume than odour 2, an ester with a fruity note.

As a first step to quantitatively examine whether sniff traces contained odour information, we compared correlations between sniff traces (after baseline correction) from trials with the same odour with correlations between sniff traces from trials with different odours, to determine whether the correlation between sniffs was higher for trials containing the same odour. Indeed, we observed, in all participants, a significantly higher sniff correlation for trials containing the same odour compared with trials containing different odours ($r_{\text{same}} - r_{\text{diff}} = 0.09$, mean participant; $P = 0.000$ for each participant, $N = 4,560$ trials for participant S1 and $N = 4,320$ trials for participants S2 and S3; two-tailed Wilcoxon rank-sum test) (Fig. 1c). We then considered sniffs grouped by perceptual ratings. Specifically, we qualitatively examined whether sniffs were distinct for trials that differed in levels of perceptual descriptors (for example, high degree of fruitiness versus low degree of fruitiness), by comparing average sniff traces that fell in the top and bottom decile of certain descriptors (Fig. 1d). We observed

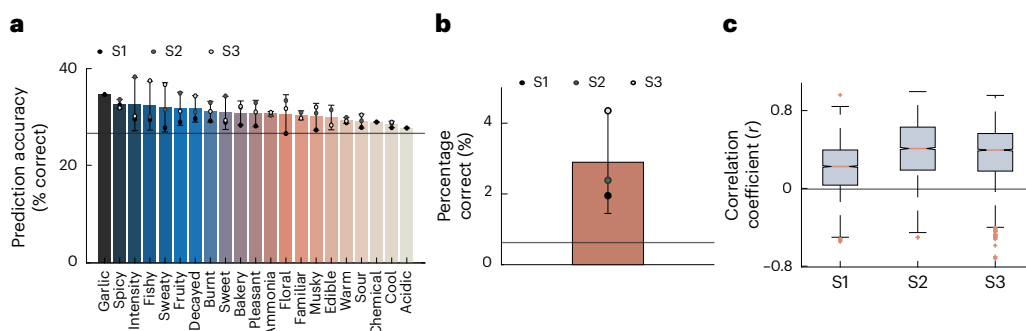


Fig. 2 | Decoding of perceptual and odour-specific information from sniffs.

a, Performance of a multilogistic regression model for each descriptor, predicting discretized ratings (low, medium and high) of a perceptual descriptor on a trial, given the sniffing parameters. Model performance was significant for most descriptors (chance correct 33.34%, $P < 0.05$, for all descriptors and participants except musky ($P = 0.114$) and floral ($P = 0.531$) in S1, one-tailed binomial test (FDR corrected), $N = 4,560$ trials in S1 and $N = 4,320$ trials in S2 and S3). Data are presented as mean values, and error bars indicate 95% CI. **b**, Decoding accuracy (percentage of trials reported correctly) of a multiclass SVM model that predicts (out of sample) odour identity based on the features of the sniff at each trial. Decoding was significant for all participants (mean participant: classification performance 2.86%, $P = 0.000$, one-tailed weighted z -test; all participants: $P = 0.000$; one-tailed z -test; $N = 4,560$ (S1), $N = 4,320$ (S2 and S3)). This decoding was also significant based on raw sniff traces (Extended Data Fig. 1), in three additional participants for group-level analyses (Extended Data Fig. 4) and based on odours with lower prediction accuracies (Extended Data Fig. 5). Data

are presented as mean values, and error bars indicate 95% CI. **c**, Distribution of correlation of perceptual ratings between the odour predicted by the classifier in **b** and the correct odour, for trials on which the decoder made a wrong prediction. This correlation was significant in each participant (S1: $r_{\text{SVM}} = 0.206$, $P = 0.000$, $N = 4,480$ trials, two-tailed Wilcoxon signed-rank test; S2: $r_{\text{SVM}} = 0.383$, $P = 0.000$, $N = 4,132$ trials, two-tailed Wilcoxon signed-rank test; S3: $r_{\text{SVM}} = 0.355$, $P = 0.000$, $N = 4,229$ trials, two-tailed Wilcoxon signed-rank test). Furthermore, this correlation was significant after accounting for mean correlation (r_{mean}) of perceptual ratings among the odours in S2 ($r_{\text{SVM}} - r_{\text{mean}} = 0.030$, $P = 0.000$, $N = 4,132$ trials, one-tailed permutation test) and S3 ($r_{\text{SVM}} - r_{\text{mean}} = 0.017$, $P = 0.000$, $N = 4,229$ trials, one-tailed permutation test) but not S1 ($r_{\text{SVM}} - r_{\text{mean}} = 0.003$, $P = 0.328$, $N = 4,480$ trials, one-tailed permutation test). See Extended Data Fig. 1 for intensity and pleasantness controls. The centre lines denote the median, the box limits denote the upper and lower quartiles, the whiskers are 1.5× interquartile range and points are outliers.

obvious differences in sniff traces for high and low values of several descriptors (for example, ‘sweaty’ across all three participants), with less obvious but still apparent differences in the sniff traces for many of the descriptors (for example, ‘fishy’ for S1 and S3) (Fig. 1d).

Perceptual and odour-specific information is contained in sniffs

To quantitatively determine whether sniffs were distinct for different levels of a perceptual descriptor, we used a multilogistic regression analysis. We first characterized each sniff trace along 24 respiratory parameters using the BreathMetrics toolbox³⁷ (Methods and Extended Data Fig. 2). We then used these parameters to predict whether a particular sniff trace was likely to belong to low, medium or high values—defined by a tercile split—of a participant-specific perceptual descriptor. For most perceptual descriptors, sniffing parameters could significantly predict the level of a perceptual descriptor for a given trial (chance correct 33.34%, $P < 0.05$, for all descriptors and participants except musky ($P = 0.114$) and floral ($P = 0.531$) in S1, binomial test (false discovery rate (FDR) corrected), $N = 4,560$ trials in S1 and $N = 4,320$ trials in S2 and S3) (Fig. 2a). Here, we used participant-wise perceptual ratings, although it is worth noting that the results were qualitatively similar, if less robust, when using either group ratings averaged across participants, or ratings from the DREAM dataset^{38,39} (Extended Data Fig. 3). This suggests that, while there is some cross-participant generalizability in the relationship between perceptual features of odours and sniffing behaviour, the effect is primarily driven by individual-level associations between personal perceptual experiences and corresponding sniffing responses. This result is in line with prior work showing that odour perception is highly individual⁴⁰.

Thus, perceptual features of odours can be decoded from sniffing behaviour alone. Because this set of perceptual descriptors can be used to uniquely identify an odour in a multidimensional space, this suggests that odour identity should also be decodable from sniffs. We therefore next performed an odour-identity decoding analysis in which we used a multiclass support vector machine (SVM) to classify which odour was presented on a given trial, based on the sniffing parameters. The

decoding performance was significant for all participants, indicating that odour identity information is embedded in sniff traces (mean classification 2.86%, chance 0.625%, $P < 0.001$, one-tailed Stouffer's z -test, $N = 4,560$ (S1), $N = 4,320$ (S2 and S3); $P = 0.000$ all participants, $N = 4,560$ trials (S1), $N = 4,320$ trials (S2 and S3)) (Fig. 2b). Critically, when the decoder made an incorrect prediction, it reported odours that were perceptually similar to the correct odour (as defined by the fine-grained feature space), indicating that olfactory perceptual information plays a key role in mapping sniff patterns to odour identities (Fig. 2c).

To further probe the relationship between perceptual features and sniffs, we next performed a representational similarity analysis (RSA) in which we compared the correspondence between odour perceptual features and sniff shapes with the correspondence between odour stimulus identity and sniff shape. To do this, we created a trial-wise similarity matrix based on similarity in perceptual ratings, and a trial-wise similarity matrix based on odour identity, describing whether the same odour was delivered in the two trials. We next examined the overlap of these similarity matrices with a third similarity matrix based on correlations of sniff traces between pairs of trials (Fig. 3a). Both the perceptual and odour-identity representational similarities were significant ($P = 0.000$, inverse-variance-weighted pooled t -test, N = all unique pairs of 4,560 (S1) and 4,320 (S2 and S3) trials) (Fig. 3b), and perceptual representational similarity exceeded odour identity representational similarity ($P = 0.000$, inverse-variance-weighted pooled t -test, N = all unique pairs of 4,560 (S1) and 4,320 (S2 and S3) trials). These results were significant even after accounting for intensity and pleasantness ($P = 0.000$, inverse-variance-weighted pooled t -test, N = all unique pairs of 4,560 (S1) and 4,320 (S2 and S3) trials), which are already known to modulate sniffs in stereotyped ways^{13,41}. Thus, fine-grained perceptual information about odours is contained in sniffs.

Perceptual and odour-specific information in sniff traces is maximal following sniff peak

Having established that fine-grained perceptual odour information is embedded in sniff traces, we next sought to understand how this

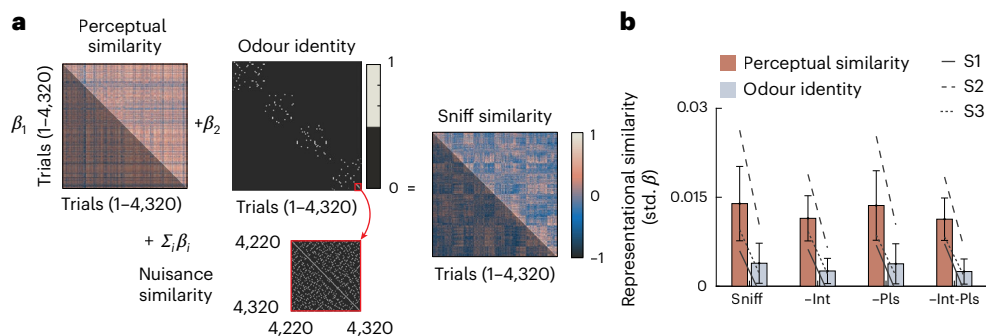


Fig. 3 | Representational similarity analyses. **a**, For each participant, we computed a perceptual similarity matrix—a correlation in perceptual ratings for all pairs of trials—as well as a binary odour identity similarity matrix, in which each value was one if and only if two trials belonged to the same odour, and zero otherwise. These matrices were regressed (along with several nuisance regressors) to predict the sniff similarity matrix, based on distance among sniffing parameters for pairs of trials. This analysis was repeated after accounting for similarity in intensity and pleasantness ratings by adding similarities in intensity and/or pleasantness as additional nuisance regressors. Σ denotes weighted summation of nuisance similarity matrices. **b**, Regression coefficients (standardized β (std. β) values) were significant in all participants for perceptual similarity (average participant: $P = 0.000$, one-tailed inverse-variance-weighted pooled t -test, N = all unique pairs of 4,560 (S1) and 4,320 (S2 and S3) trials). Furthermore, there was a small but significant representational similarity for odour identity, beyond perceptual similarity (mean participant: $P = 0.000$,

one-tailed inverse-variance-weighted pooled t -test, N = all unique pairs of 4,560 (S1) and 4,320 (S2 and S3) trials). These findings were similar when we used permutation tests and shuffled odour identities across trials before constructing RSMs (average participant: $P = 0.000$, one-tailed permutation tests, N = all unique pairs of 4,560 (S1) and 4,320 (S2 and S3) trials, percentile of actual RSA coefficients in relation to the null distribution; Methods). These effects were robust when accounting for similarity in intensity (-Int), pleasantness (-Pls) and both intensity and pleasantness (-Int-Pls) ($P = 0.000$, one-tailed inverse-variance-weighted pooled t -test, N = all unique pairs of 4,560 (S1) and 4,320 (S2 and S3) trials). Data are presented as mean values, and error bars indicate s.e.m. across participants. See Methods for details on combining RSA regression weights and standard error across participants using an inverse-variance-weighted estimate to yield a single pooled t -statistic (and P value). For all RSA analyses, N = all unique pairs of trials out of 4,560 trials in S1 and 4,320 trials in S2 and S3, that is, $N = 10,394,520$ (S1) and 9,329,040 (S2 and S3).

relationship evolves over time within a sniff cycle. To this end, we adapted the sniff similarity RSA in Fig. 3b, by performing temporal unwrapping in which sniff similarity was constructed on the basis of the raw flow rates at each timepoint of the sniff cycle (every 100 ms) (Fig. 4a).

This analysis revealed a temporal profile of perceptual information, where maximal perceptual information was contained not at the peak nasal airflow, but rather ~500 ms after the peak (Fig. 4b). Plotting the temporal RSA alongside the participant-averaged airflow revealed distinct phases in the mutual relationship between their temporal profiles. Initially, both perceptual information in the sniff and airflow increased; this was followed by a phase in which airflow decreased while perceptual information continued to rise. Subsequently, both measures showed a consistent decline, eventually returning to baseline (Fig. 4c). This pattern contained idiosyncratic components but showed some consistency across all participants (Fig. 4d). Importantly, these results remained significant after accounting for intensity and pleasantness (Extended Data Fig. 6).

Neural basis of perceptual modulation of sniffs

Because fine-grained perceptual odour information can be extracted from sniffing parameters, and these olfactory-based sniff modulations likely require cortex^{17,22,42}, we next sought to identify the neural substrates of percept-driven sniff modulations, with a focus on the major olfactory cortical regions^{43,44}. These included piriform cortex, amygdala, orbitofrontal cortex (OFC), olfactory tubercle and anterior olfactory nucleus (Fig. 5a). It is already well established that sniffing and breathing alone activate all major olfactory cortical areas^{1,4,11,45–49}, and, as expected, this effect was evident in our data (Fig. 5b–e). However, our goal here was not limited to identifying brain areas whose activity was broadly modulated by sniffs, but rather identifying brain areas whose activity represented aspects of the sniff that were modulated by perceptual properties of the odour. To achieve this, we adapted the RSA in Fig. 3b to examine neural representations of aspects of the sniff that were modulated by perceptual information. Specifically, we performed cluster averaging of sniff traces

in three different configurations and measured the correlation of cluster-by-cluster sniff similarities with the corresponding neural similarities (Fig. 5b,c). The three clustering configurations performed on the sniffing data were: (1) sniff-shape clustering: grouping sniff traces based on their overall shape with no consideration of the odours being sniffed, to extract aspects of sniffs that are independent of olfactory perceptual information; (2) perceptual-sniff-modulation clustering: grouping sniff traces based on the perceptual features of the odours being sniffed with no consideration of the overall sniff shape, to extract the aspects of sniffs that are common to similar olfactory perceptual features, independent of the overall shape of the sniff; and (3) random clustering of sniff trials as a statistical control since lack of variance among the clusters should elicit no representational similarity (Fig. 5c). As expected, we found that sniff-shape clustering corresponded to neural activity in all olfactory cortical areas ($P = 0.000$ all areas, inverse-variance-weighted pooled t -test, N = all unique pairs of 4,560 (S1) and 4,320 (S2 and S3) trials) (Fig. 5d), with a smaller subset of regions also containing representations of perceptual-sniff-modulation clustering ($P = 0.000$ all areas except piriform cortex: $P = 0.003$, inverse-variance-weighted pooled t -test, N = all unique pairs of 4,560 (S1) and 4,320 (S2 and S3) trials) (Fig. 5d,e). Specifically, across all voxels that contained neural representations of sniff shape, there was a subset that contained representations of perceptual sniff modulation, mainly in the amygdala (Fig. 5e, orange areas, with a small additional cluster in the OFC). However, given that perceptual and sniffing information are related (Figs. 2–4), it is conceivable that schemes for sniffing and perceptual clustering are not independent. Therefore, we performed an additional control analysis in which we implemented an iterative clustering orthogonalization algorithm (Methods) to ensure that the clustered matrices had minimal overlap. Crucially, these results were robust to orthogonalization of the clustered matrices, such that the perceptual-sniff-modulation clustering captured exclusively perceptual information, with no residual sniff-shape information (Extended Data Fig. 8). Furthermore, these results were robust to exclusion of intensity and pleasantness (Extended Data Fig. 8). While these results helped to identify brain

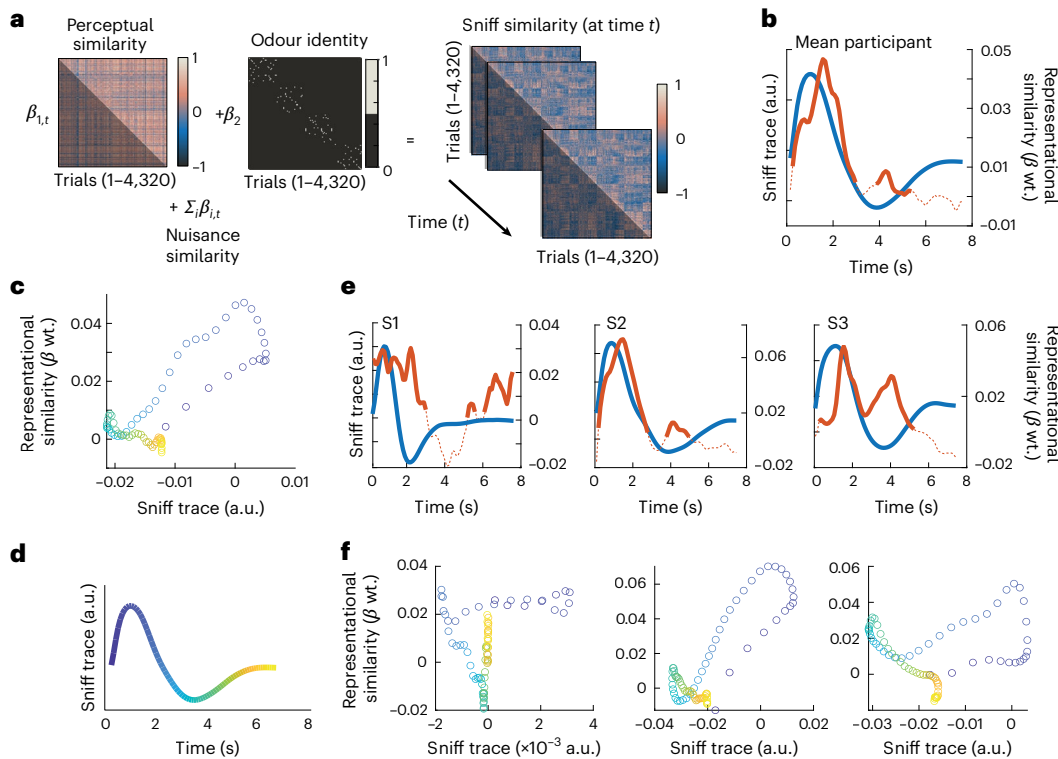


Fig. 4 | Temporal RSA. **a**, For each participant, a perceptual similarity matrix was computed as the correlation in perceptual ratings for all pairs of trials, as well as a binary odour identity similarity matrix, in which each value was one if and only if two trials belonged to the same odour, and zero otherwise. These matrices were regressed (along with several nuisance regressors) to predict the sniff similarity matrix based on distance of sniff flow rate for a pair of trials at each timepoint of the sniff cycle. Σ denotes weighted summation of nuisance similarity matrices. **b**, The temporal profile of perceptual similarity regression coefficients (std. β weights (β wt.), orange) overlaid on the sniff flow temporal profile (blue), averaged across participants. Solid lines indicate the timepoints at which the regression coefficient was significant ($P < 0.05$, participant-wise one-tailed t -test, on β wt. shown in **e** for at least two of three participants), and dashed lines denote otherwise. The RSA peak is 500 ms after peak sniff flow. **c**, Perceptual representational similarity in **b** plotted as a function of sniff flow rate. **d**, Colour-coded sniff cycle corresponding to colours shown in **c** and **f** (100-ms timepoints).

e, Temporal perceptual representational similarity as in **b**, but for individual participants. Solid lines indicate the timepoints at which the regression coefficient was significant ($P < 0.05$, FDR corrected across time bins, one-tailed t -test, N = all unique pairs of 4,560 (S1) and 4,320 (S2 and S3) trials: 10,394,520 (S1) and 9,329,040 (S2 and S3)) in each individual participant, and dashed lines denote otherwise. The RSA peak occurred after peak sniff flow at 1,300 ms for S1, 500 ms for S2 and 400 ms for S3. Information peaks varied across participants, but were always confined to the first 2 s of the sniff cycle when distinct samples of odours were taken for analysis (Extended Data Fig. 7). **f**, Perceptual similarity plotted as a function of sniff flow for individual participants. There was no consistency in specific descriptors being more prominent for time-series RSAs across all participants (Extended Data Fig. 7). All participant-wise results were corrected for multiple comparisons across time bins by FDR correction (Benjamini–Hochberg procedure).

areas underlying olfactory-percept-based modulation of sniffs, they did not quantify the richness or dimensionality of the perceptual information embedded in the sniff modulations. It is possible that for some regions the sniff coding is modulated by a rich spectrum of perceptual descriptors, while for others the modulation is based on relatively fewer descriptors. To explore this, we adapted the RSA in Fig. 5d to compute percept-wise clustering of sniffs, and implemented the clustered RSA similar to Fig. 5b, but based on clustering the trials for each individual perceptual feature separately. In other words, the clustering of trials based on perceptual descriptors was performed separately for each descriptor, yielding as many representational similarity coefficients as the number of descriptors. We then counted the number of perceptual features for which a specific voxel had significant clustered representational similarity ($P < 0.05$, one-tailed t -test, N = all unique pairs of 4,560 (S1) and 4,320 (S2 and S3) trials). This metric was the highest for amygdala ($F_{4,10132} = 108.651$; $P = 0.000$, repeated-measures analysis of variance (ANOVA)) (Fig. 5f,g), indicating that the amygdala, especially its more medial and cortical subregions, best captures aspects of sniffs that are modulated by perceptual information. Notably, these results were similar after exclusion of intensity and pleasantness (Extended Data Fig. 9).

Discussion

Sniffing and odour processing are inextricably linked. Elegant work has established that sniff volumes are altered in response to odour intensity and pleasantness^{13,41}, but whether fine-grained perceptual and odour identity information is embedded in sniffing behaviour has been unknown. Olfactory perceptual responses are highly individual, so much so that perception can form an olfactory fingerprint unique to each individual⁴⁰. Thus, addressing this question required precise measures of sniffing in response to a large number of odours from individual participants. Here, we took advantage of an existing dataset^{30,36}, in which human participants smelled 160 odours over at least 4,320 trials, to probe the intricate relationship between odour perception and sniffing. We show that the perceptual qualities of odours can modulate sniffing behaviour in a nuanced manner. While the overall effect sizes of the modulation were small, this is unsurprising because sniffing is also impacted by a range of homeostatic, autonomic and behavioural factors. Despite these complex factors, a consistent effect of fine-grained perceptual features of odour—and even odour identity—on sniffing behaviour emerged across participants, demonstrating that odour coding is related to its sampling motor behaviour in a percept-specific manner. This, in turn, shows that in olfaction, similar to other modalities, there is a feedback mechanism subserving

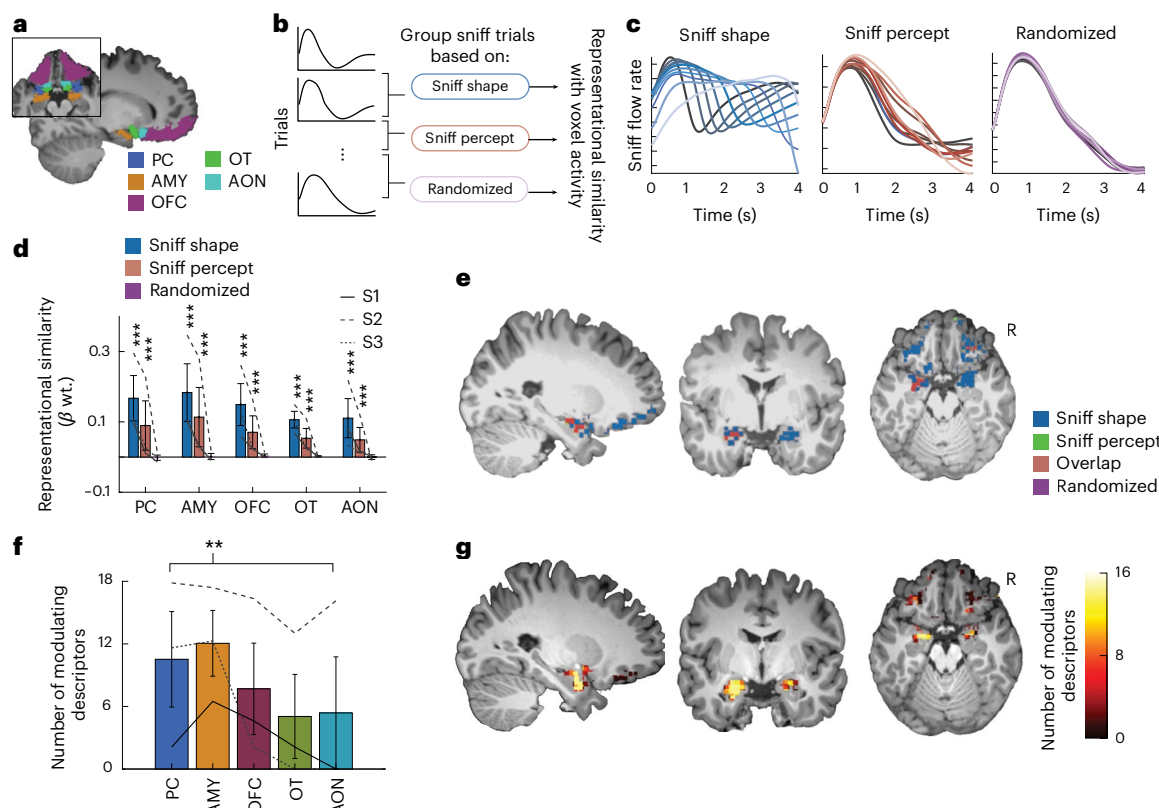


Fig. 5 | Neural basis of perceptual modulation. **a**, Olfactory ROIs: piriform cortex (PC), amygdala (AMY), OFC, olfactory tubercle (OT) and anterior olfactory nucleus (AON). **b**, Schematic of clustered RSAs in which we averaged sniff traces across trials with similar sniff shape (sniff shape), similar perceptual profiles (sniff percept) or randomly (randomized) (as control), before performing RSA with similarly grouped fMRI data. See Methods for details. **c**, Average traces when trials were clustered based on sniff shape (left), sniff percept (middle) and randomized (right). **d**, Regression coefficients of sniff shape, sniff percept and randomized clustered sniff similarity matrices with correspondingly clustered neural data. Regression coefficients of raw sniffing parameters based on sniff shape were significantly higher than the random control ($P = 0.000$, all areas, one-tailed inverse-variance-weighted pooled t -test, $N = \text{all unique pairs of } 4,560 \text{ (S1) and } 4,320 \text{ (S2 and S3) trials: } 10,394,520 \text{ (S1) and } 9,329,040 \text{ (S2 and S3)}$). Similarly, regression coefficients of sniff percept clustering were significantly higher than the random control ($P = 0.000$, all areas, except AON; $P = 0.003$, one-tailed inverse-variance-weighted pooled t -test, $N = \text{all unique pairs of } 4,560 \text{ (S1) and } 4,320 \text{ (S2 and S3) trials: } 10,394,520 \text{ (S1) and } 9,329,040 \text{ (S2 and S3)}$). **e**, Searchlight analyses to indicate where

representations of sniff shape, sniff percept and randomized clustering of sniff responses were significant in at least two of three participants ($P < 0.05$, two-tailed t -test, FDR corrected). Raw sniff information (sniff shape, blue) was pervasive throughout olfactory regions. A subset of these regions captured aspects of sniff information modulated by perceptual features (sniff percept, red for voxels overlapping with raw sniff voxels; otherwise, green). **f**, Number of perceptual features for which clustered RSA was significant across regions (averaged across all odour-responsive voxels at threshold $P = 0.05$, one-tailed t -test, $N = \text{all unique pairs of } 4,560 \text{ (S1) and } 4,320 \text{ (S2 and S3) trials: } 10,394,520 \text{ (S1) and } 9,329,040 \text{ (S2 and S3)}$). Number of significantly modulating features was highest in the AMY ($F_{4,10132} = 108.651$; $P = 0.000$, repeated-measures ANOVA; $P = 0.000$ for post hoc comparison between AMY and other anatomical regions, except PC; $P = 0.019$, pairwise t -test, FDR corrected). **g**, Searchlight-based clustered RSA showing the number of perceptual features for which the clustered RSA was significant in at least two of three participants ($P < 0.05$, one-tailed t -test). Data are presented as mean values, and error bars indicate the s.e.m. across participants in **a–g**. *** $P < 0.001$; ** $P < 0.01$.

active sensing as was previously hypothesized¹³. In vision, for example, information is systematically acquired through eye movements, including rapid saccades, and is related to cognition and attention^{50,51}. This motor sampling scheme contains reliable information regarding the location and timing of the gaze^{52,53}. Furthermore, visual motor information can be used to predictively modify neural activity to fine-tune stimulus coding based on the context and task^{53–55}. Active sensing has also been observed in the somatosensory^{56,57} and auditory⁵⁸ systems.

Similarly, in olfaction, sniff modulations may underlie optimization of the timing of sampling the chemical stimulus^{1,7,11}. This is intriguing, especially given the lack of spatial information contained within sniffs, and suggests that, in line with previous animal work^{7,46}, timing is an important component of the olfactory code¹. Furthermore, recent single-unit recordings sharpen this picture⁵⁹, showing that piriform and medial-temporal lobe regions follow distinct temporal profiles during odour evaluation. It is conceivable that early olfactory cortical regions such as piriform cortex and amygdala may trigger feedback to

shape ongoing airflow, while later limbic regions and the OFC update the loop based on emerging perception. Indeed, recent work shows that the piriform cortex sends rapid feedback to the olfactory bulb⁶⁰. In light of this, our findings further suggest that precise modulations of nasal airflow could potentially constitute predictive information used by the olfactory system to improve perceptual acuity.

We observed that perceptual information was maximally imbedded in sniffs approximately 500 ms after peak airflow through the nose, not at the time of peak flow. Interestingly, this is substantially later than the earliest time at which sniffs can be modulated through this neural feedback mechanism, which is around 200 ms after sniff onset¹³. One potential explanation for this could be that most odours activate two interacting but distinct systems for chemical processing, namely the trigeminal and olfactory systems^{61,62}. Similar to the olfactory system, the trigeminal system is known to influence sniffing behaviour⁶³. Animal work in decerebrated rodents shows that trigeminal-based sniff modulations may happen in perfused brainstem preparations

in the absence of cortical control¹⁷, suggesting that trigeminal-based sniff modulations mediated by the brainstem may occur faster than olfactory-perception-based modulations requiring cortex. In this way, early sniff modulations may optimize certain coarse perceptual features of odours such as intensity and pleasantness^{64–66}, whereas later sniff modulations may optimize other fine-grained features that can be mapped to precise odour identities. However, it is important to note that we did not explicitly acquire trigeminality ratings for the odours and therefore, we are unable to examine whether trigeminality had a consistent effect on sniffs.

We also explored neural substrates underlying sniff modulations based on odour perceptual information. These substrates probably span multiple brain areas, including both cortical and subcortical regions. We focused here on cortical substrates and found that the correspondence between odour-percept-related sniff modulations and neural activity was maximal in the amygdala. This included rostral amygdala areas that overlap with the olfactory amygdala⁶⁷, which receive direct input from the olfactory bulb^{68–70} and preserve a chemotopic map^{71,72}. Interestingly, these results are also compatible with findings in epilepsy research in which the amygdala has been considered a key respiratory control area^{18–21}. In patients with epilepsy, spread of seizures to amygdala causes apnoea, and stimulation of the amygdala disrupts breathing^{20,21}. Furthermore, the amygdala is known to project to respiratory nuclei in the brainstem^{22,23}. The possibility that olfactory amygdala subregions may underlie odour-percept-driven sniff modulations dovetails with this prior work and may extend our understanding of the role of the amygdala in respiratory control.

While these results shed light on the close relationship between sniffing and perceptual information, as well as the neural basis of this interaction, our reliance on trial-averaged blood oxygenation level-dependent responses and airflow traces necessarily blurs rapid, sniff-phase-locked fluctuations and intertrial variability that single-trial approaches can reveal⁷³. Furthermore, we did not trace the temporal dynamics of neural markers of odour-percept-related sniff modulations because of the slow timescale of haemodynamic responses. Notably, we used a dataset optimized for signal detection in olfactory cortical areas; thus, our findings are limited by restricted regional coverage. We therefore did not explore several brain regions such as the brainstem^{22,23} and cerebellum⁷⁴ that may be linked to involuntary sniff control. By focusing on olfactory brain regions and examining the neural responses linked to odour-percept-based sniff modulations across time, we provide evidence of a role for the amygdala in implementing a feedback mechanism that modulates nasal airflow in response to chemical stimuli.

Methods

Human participants

Data were obtained from the Neural Encoding Models of Olfaction (NEMO) dataset³⁶, described in detail in ref. 30, comprising three human participants (two females aged 23–24 years, one male aged 24 years). Additional data were acquired for group-level analysis consisting of three additional participants (two females aged 28 and 30 years, one male aged 44 years). All participants were compensated for their participation consistent with institutional review board (IRB)-approved protocols (NEMO Data IRB: STU00205961; follow-up behavioural experiment IRB: STU00201747). This study was approved by the IRB at Northwestern University and adhered to the Declaration of Helsinki and the Belmont Report. Participation was voluntary, and written informed consent was obtained from all participants.

Dataset description

Here, we used fMRI data, nasal airflow recordings and behavioural ratings from 3 healthy human participants while they smelled 160 monomolecular odours across 4,560 (S1) or 4,320 (S2 and S3) trials. Stimuli were presented inside the scanner across 12 sessions (~18 h)

per participant. For each trial in the scanner, each participant rated the odour on one of the 18 perceptual descriptors. The descriptors used were: pleasantness, intensity, fishy, burnt, sour, decayed, musky, fruity, sweaty, cool, floral, sweet, warm, bakery and spicy. S1 also rated acidic, garlic and chemical-like, whereas S2 and S3 rated ammonia, edibility and familiarity. Participants S2 and S3 also rated the odours on the same perceptual descriptors outside the scanner during a self-paced behavioural task. Breathing was measured using a breathing belt (S1) or a pneumotachometer and spirometer (S2 and S3).

The fMRI data were acquired at 3 T using gradient echo T2*-weighted EPI at a resolution of 2 mm isotropic for S1 and 1.7 mm in-plane and 2 mm slice thickness for S2 and S3 and a repetition time of 1.4 s for all participants. We used the Friston-24 as nuisance regressors⁷⁵, based on translation and rotation parameters estimated during the realignment. Single-trial voxel responses were estimated using the GLMsingle toolbox^{76,77} that fits custom haemodynamic response functions for each voxel in addition to denoising and fractional ridge regression. Breathing and sniffing traces were not regressed out from the neural data analysis as nuisance regressors.

Using an fMRI acquisition optimized for key olfactory cortical regions, we focused on olfactory regions of interest, namely the piriform cortex, amygdala, OFC, anterior olfactory nucleus and olfactory tubercle. Other regions that receive olfactory input, including the lateral entorhinal cortex, can be odour responsive in some contexts. We did not observe consistent and robust odour responses in the lateral entorhinal cortex across participants, although our scanning acquisition window may have precluded consistent detection in this area. Region of interest (ROI) masks were inversely normalized to each participant's T1 images. Grey matter odour-responsive voxels in each ROI were used for all analyses.

Characterizing the sniff time series

We first transformed the breathing belt data to airflow units by smoothing and performing a temporal derivative on the trace. We validated this transformation using several sessions collected from participant S2 that included simultaneous measurements from both the breathing belt and the spirometer (Extended Data Fig. 10).

We examined the sniff time series for each trial by first creating epochs beginning at the sniff cue and extending for 5 s. To ensure accuracy of sniff onsets relative to the sniff cue, we manually parsed through all trials across all participants confirming that the peak sniff flow corresponded to segments of the sniff following the cue. Next, we used the BreathMetrics toolbox³⁷ to parametrize the sniff traces, extracting 12 features from each trace. We created 12 additional composite sniffing parameters based on the ones provided by the BreathMetrics toolbox, further describing aspects of the sniff around critical points such as peak inhale and exhale trough. The features have been summarized in Supplementary Table 1 and shown in Extended Data Fig. 2.

Multilogistic regression model

We used a multilogistic regression model to map sniffs to participant-wise odour percepts. The regression analysis was computed on participant-wise perceptual ratings. On each trial, the participant smelled one odour and was then asked to rate that odour on a single perceptual descriptor to maximize the accuracy of the ratings. The descriptor to be rated was randomly selected for each trial such that, over the course of all trials of that odour, we obtained a complete set of ratings across all perceptual descriptors; every odour was rated on every descriptor. In this analysis, for each participant, ratings were averaged across the subset of trials that included a rating of that descriptor. After parameterizing sniffs along various features for each trial, we used them to predict whether a particular sniff trace was likely to belong to low, medium or high values of a participant-specific perceptual descriptor. Low, medium and high values of a descriptor were based on whether the odour in that trial belonged to the lowest, middle

or highest tercile of all ratings for that descriptor for that participant. Statistical analyses were performed for each descriptor and participant separately (binomial test, with 1/3 chance, FDR correction across all comparisons per participant, $N = 4,560$ trials for S1 and $N = 4,320$ trials for S2 and S3). In addition, we repeated the analysis using only the group-wise ratings or the DREAM dataset^{38,39}.

Decoding odour identity from sniffs

We used a multiclass SVM to decode odour identity from sniff parameters. First, we performed a principal component analysis on sniff parameters to extract the optimal number of principal components that explained at least 90% of variance in the data. We then used these components as features in our SVM to predict the odour presented on each trial. We used the SVM with the following specifications:

We performed a fourfold cross-validation and computed the prediction accuracy as the number of trials for which the out-of-sample prediction was correct. We then repeated this analysis based on raw sniffing parameters without feature extraction. We assessed the significance of classification performance across n classes using a binomial test, where the probability of success for each class occurs as $1/n$ due to the evenly distributed chance of selecting any one of the n odours. The variance of the number of accurate predictions, $\text{Var}(\text{SVM}_n)$, according to the binomial distribution, is given by $N(\frac{1}{n}(1 - \frac{1}{n}))$, where N is the total number of samples and n is the number of classes (or number of odours). Consequently, the standard deviation of the normalized accuracies is calculated as $\sqrt{\text{Var}(\text{SVM}_n)/N^2} = \sqrt{\frac{1}{n}(1 - \frac{1}{n})}/N$. We then transformed the observed accuracy into a z score and computed the P values based on this z statistic.

Furthermore, we examined the trials for which the SVM made a wrong prediction. We asked if, for those trials, the predicted odour was perceptually related to the correct odour by taking a Pearson's correlation of perceptual ratings between the predicted and correct odour. We measured the significance of this correlation using a Wilcoxon signed-rank test to quantify if the median correlation across all wrongly classified trials was significantly higher than zero. Furthermore, we performed a permutation test to account for baseline correlation among perceptual ratings of odours. As a control, we also considered correlations of ratings for predicted and correct odours without including intensity and pleasantness.

RSA of sniffs

We performed RSA to determine whether perceptual information about odours and their precise identity is represented in the sniffs. Similar to the 'Decoding odour identity from sniffs' section, we reduced the dimensionality of sniff feature space using principal component analysis and selected principal components that cumulatively explained at least 90% of the variance. We created the representational similarity matrices (RSMs) for sniffs across trials based on the correlation of principal components of sniff features for all pairs of trials. We also created perceptual similarity matrices based on correlation of perceptual ratings for pairs of trials. In addition, we created a binary odour identity similarity matrix based on whether two trials belonged to the same odour. We also created various nuisance regressor matrices specifying whether two odours belonged to the same run, session or set of odours. As controls, we repeated the RSA with sniff RSM based on both raw sniff traces and perceptual ratings, including all descriptors except intensity and pleasantness.

We measured the significance of the regression coefficients using a t -test within each participant ($N = \text{number of pairs of trials per participant}$). We also performed a weighted average of regression coefficients across participants based on the inverse of squared standard errors. We then combined the participant-wise t value of the combined regression coefficients based on the combined standard error and the smallest of the degrees of freedom among the participants, to obtain the group statistic for the mean participant. We further verified this by performing a

permutation test wherein we regressed the sniff similarity matrix (and nuisance matrices) against the shuffled perceptual similarity matrix, yielding a null distribution of RSA coefficients when repeated 1,000 times for each participant. The P value was then estimated by computing the percentile of actual (unshuffled) RSA coefficients in relation to the null distribution. Notably, no comparisons were needed in this analysis because the hypotheses for all the cases were independent of each other (for example basic RSA, RSA controlling for intensity, pleasantness and so on).

Temporal representational similarity

We adapted the RSA described above to probe the representation of perceptual information in sniffs separately at timepoints across the sniff time series, at intervals of 100 ms. We defined the time-wise sniff RSM as the negative absolute difference between the raw sniff response for all pairs of trials at the same instant of time. Next, similar to the time-invariant version of the RSA in Fig. 3, we regressed the perceptual RSMs against the sniff RSMs to obtain an estimate of the extent to which the perceptual information of odours overlapped with the sniff-related information. This allowed us to visualize the temporal evolution of the representation of perceptual information in the sniffs. The statistical analyses were similar to the time-invariant RSA. To characterize various phases in the temporal evolution of representational similarity, we plotted the regression coefficient of perceptual similarity as a function of amplitude of sniff for the same time bin.

To examine the variability of timing in the peak representational similarity information, we also performed the analysis across 100 bootstraps, each with a distinct population of odours. Furthermore, to consider whether specific perceptual descriptors were dominant in the temporal RSA, we repeated this analysis with a perceptual similarity matrix constructed exclusively on a single perceptual descriptor. In other words, the perceptual similarity for two trials on a single descriptor (for example, pleasantness) corresponded to the absolute difference in values (for example, in pleasantness) for the odours delivered on the two trials. Notably, we did not explicitly acquire trigeminality ratings for the odours and were therefore unable to determine whether the trigeminal component of odours had a qualitatively distinct impact on the sniff time series. These analyses are described in Extended Data Fig. 7.

RSA for neural data

To determine whether the percept-based sniff modulations were represented in the neural data, we implemented a variant of the RSA described above. We averaged sniffs across trials in different ways to isolate different influences on the variability in sniffs. Specifically, we isolated sniff variability that was largely independent of perceptual information, as well as sniff variability that was dependent on perceptual information. To do this, we performed clustering analyses in which we grouped trials based either solely on the similarity of the sniff shape (sniff-shape-based sniff-modulation clustering) or solely on the similarity of the percept of the odour presented (percept-based sniff-modulation clustering). For sniff-shape-based clustering, we used a k -means clustering algorithm with squared Euclidean distance to cluster the trials. We then cluster-averaged the voxel responses with the same clustering index and performed RSA based on cluster-by-cluster RSMs of sniff and neural responses. This way of clustering prioritizes examining the representation of all sniff-shape-related information largely irrespective of perceptual information. For the percept-based sniff-modulation clustering, we performed a clustering analysis on odour perceptual ratings, such that the trials that belong to perceptually similar odours were grouped in the same cluster. We averaged the sniffs and neural responses using this perceptual clustering scheme. We next performed RSA to map the sniffs grouped based on perceptual information (in other words, the sniff modulations) to neural data. This clustering approach prioritizes examining the representation of

all percept-related information embedded within the sniffs. We then performed a null clustering analysis in which we randomly clustered the sniff trials without considering percept or sniff shape. We used the same number of clusters (60) for all clustering approaches and across all participants. The choice of the number of clusters was based on the elbow method, which identifies the optimal number of clusters as the point where the within-cluster sum of squares shows a marked decrease. We computed these representational similarities for searchlights of voxels across brain areas. We then averaged the regression coefficients across searchlights in the same brain areas.

We extended this clustered RSA approach to examine modulations of sniffs based on specific perceptual descriptors. In other words, we clustered the sniff and neural responses based on clustering of individual perceptual descriptors. For each voxel, we computed the number of descriptors for which the representational similarity for the clustered sniffs was significant. To compare the number of modulating descriptors across ROIs, we used a mixed-effects ANOVA in which the ROIs corresponded to the fixed effects and the participants corresponded to random effects. We then performed post hoc tests to examine whether specific regions had a higher number of modulating descriptors than other regions.

Statistical analyses

All statistical analyses were first performed at a single-participant level in which the degrees of freedom corresponded to the number of trials per participant (4,560 (S1) and 4,320 (S2 and S3)). This included the pattern correlation analysis in Fig. 1c, multilogistic regression in Fig. 2a and all RSA analyses from Figs. 2–5. However, for summary purposes, the statistical analyses for group effects were also computed for some analyses (RSA; Fig. 3b) by using an inverse-variance-weighted pooled *t*-test as described here. For each predictor in the RSA (for example, perceptual similarity in Fig. 3b), we took each participant's β and its standard error ($SE = \beta/t$), computed an inverse-variance-weighted average β across the three participants, and then divided that weighted mean by its combined SE to yield a single, combined *t*-statistic. The resulting *t*-statistic (with degrees of freedom equal to the smallest among the three participants) was used to compute a *P* value. In other words, rather than performing a simple *t*-test on three numbers, we performed a fixed-effects meta-analysis.

Iterative clustering orthogonalization algorithm

To ensure that the sniff-shape-based and percept-based clustering schemes were independent, we implemented an additional control analysis involving a custom iterative clustering orthogonalization algorithm. We used the adjusted random index (ARI) to quantify the overlap in the two clustering schemes, that is, clustering based on sniffs and clustering based on perceptual ratings. Given the intrinsic relationship between perceptual qualities and sniffs, we initially observed a small but significant ARI. This algorithm progressively blurred the co-occurrence matrix of the two clustering schemes until the ARI between them was no longer statistically significant.

In more detail, our process began with two clustering schemes, C_1 and C_2 , representing the clustering indices for each trial. We used a probabilistic smoothing algorithm starting with the computation of a co-occurrence matrix for C_1 and C_2 , which represented the number of trials within each pairwise combination of clustering bins. We then iteratively targeted the bins (bivariate bins) with the highest number of co-occurrences—where assignment to a specific sniff cluster was highly predictive of assignment to a particular perceptual cluster, and vice versa. Trials from these maximally overlapping bins were probabilistically reassigned to other clusters that were most similar to their original assignments. This reassignment process involved considering the next six most similar clusters as potential reassignment targets. The number of clusters considered during reassignment (six in our case) corresponded to the size of the smoothing kernel. This

iterative process continued until the ARI between the newly assigned cluster identities fell below a significance threshold. In addition, we verified that the new clustering identities maintained a high ARI with their original indices. This approach ensured that knowledge of a sniff cluster no longer reliably predicted the perceptual cluster, thereby decoupling the two clustering schemes.

Reporting summary

Further information on research design is available in the Nature Portfolio Reporting Summary linked to this article.

Data availability

Analyses presented here used a previously published database^{30,36}. Additional behavioural data for group-level analyses are available via GitHub at <https://github.com/viveksgr/SFP>.

Code availability

All analyses were performed in MATLAB R2023b. Code for preprocessing and reproducing the results presented in this article is available via GitHub at <https://github.com/viveksgr/SFP>.

References

1. Kepcs, A., Uchida, N. & Mainen, Z. F. The sniff as a unit of olfactory processing. *Chem. Senses* **31**, 167–179 (2006).
2. Wachowiak, M. All in a sniff: olfaction as a model for active sensing. *Neuron* **71**, 962–973 (2011).
3. Mainland, J. & Sobel, N. The sniff is part of the olfactory percept. *Chem. Senses* **31**, 181–196 (2006).
4. Sobel, N. et al. Sniffing and smelling: separate subsystems in the human olfactory cortex. *Nature* **392**, 282–286 (1998).
5. Laing, D. G. Natural sniffing gives optimum odour perception for humans. *Perception* **12**, 99–117 (1983).
6. Cury, K. M. & Uchida, N. Robust odor coding via inhalation-coupled transient activity in the mammalian olfactory bulb. *Neuron* **68**, 570–585 (2010).
7. Verhagen, J. V., Wesson, D. W., Netoff, T. I., White, J. A. & Wachowiak, M. Sniffing controls an adaptive filter of sensory input to the olfactory bulb. *Nat. Neurosci.* **10**, 631–639 (2007).
8. Kareken, D. A. et al. Olfactory system activation from sniffing: effects in piriform and orbitofrontal cortex. *NeuroImage* **22**, 456–465 (2004).
9. Wachowiak, M. & Cohen, L. B. Representation of odorants by receptor neuron input to the mouse olfactory bulb. *Neuron* **32**, 723–735 (2001).
10. Miura, K., Mainen, Z. F. & Uchida, N. Odor representations in olfactory cortex: distributed rate coding and decorrelated population activity. *Neuron* **74**, 1087–1098 (2012).
11. Shusterman, R., Smear, M. C., Koulakov, A. A. & Rinberg, D. Precise olfactory responses tile the sniff cycle. *Nat. Neurosci.* **14**, 1039–1044 (2011).
12. Jordan, R., Fukunaga, I., Kollo, M. & Schaefer, A. T. Active sampling state dynamically enhances olfactory bulb odor representation. *Neuron* **98**, 1214–1228 (2018).
13. Johnson, B. N., Mainland, J. D. & Sobel, N. Rapid olfactory processing implicates subcortical control of an olfactomotor system. *J. Neurophysiol.* **90**, 1084–1094 (2003).
14. Prescott, J., Burns, J. & Frank, R. A. Influence of odor hedonics, food-relatedness, and motivational state on human sniffing. *Chemosens. Percept.* **3**, 85–90 (2010).
15. Ferdzeni, C., Fournel, A., Thévenet, M., Coppin, G. & Bensafi, M. Viewing olfactory affective responses through the sniff prism: effect of perceptual dimensions and age on olfactomotor responses to odors. *Front. Psychol.* **6**, 1776 (2015).
16. Johnson, B. N., Russell, C., Khan, R. M. & Sobel, N. A comparison of methods for sniff measurement concurrent with olfactory tasks in humans. *Chem. Senses* **31**, 795–806 (2006).

17. de los Cobos Pallares, F. P., Bautista, T. G., Stanić, D., Egger, V. & Dutschmann, M. Brainstem-mediated sniffing and respiratory modulation during odor stimulation. *Respir. Physiol. Neurobiol.* **233**, 17–24 (2016).
18. Dlouhy, B. J. et al. Breathing inhibited when seizures spread to the amygdala and upon amygdala stimulation. *J. Neurosci.* **35**, 10281–10289 (2015).
19. Masaoka, Y. & Homma, I. in *Post-genomic Perspectives in Modeling and Control of Breathing* (eds Champagnat, J. et al.) 9–14 (Springer, 2004).
20. Nobis, W. P. et al. Amygdala-stimulation-induced apnea is attention and nasal-breathing dependent. *Ann. Neurol.* **83**, 460–471 (2018).
21. Nobis, W. P. et al. The effect of seizure spread to the amygdala on respiration and onset of ictal central apnea. *J. Neurosurg.* **132**, 1313–1323 (2019).
22. Yang, C. F., Kim, E. J., Callaway, E. M. & Feldman, J. L. Monosynaptic projections to excitatory and inhibitory preBötzinger complex neurons. *Front. Neuroanat.* **14**, 58 (2020).
23. Trevizan-Baú, P. et al. Forebrain projection neurons target functionally diverse respiratory control areas in the midbrain, pons, and medulla oblongata. *J. Comp. Neurol.* **529**, 2243–2264 (2021).
24. Rhone, A. E. et al. A human amygdala site that inhibits respiration and elicits apnea in pediatric epilepsy. *JCI Insight* **5**, e134852 (2020).
25. Lacuey, N., Zonjy, B., Londono, L. & Lhatoo, S. D. Amygdala and hippocampus are symptomatogenic zones for central apneic seizures. *Neurology* **88**, 701–705 (2017).
26. Howard, J. D., Plailly, J., Grueschow, M., Haynes, J.-D. & Gottfried, J. A. Odor quality coding and categorization in human posterior piriform cortex. *Nat. Neurosci.* **12**, 932–938 (2009).
27. Stettler, D. D. & Axel, R. Representations of odor in the piriform cortex. *Neuron* **63**, 854–864 (2009).
28. Roland, B., Deneux, T., Franks, K. M., Bathellier, B. & Fleischmann, A. Odor identity coding by distributed ensembles of neurons in the mouse olfactory cortex. *eLife* **6**, e26337 (2017).
29. Pashkovski, S. L. et al. Structure and flexibility in cortical representations of odour space. *Nature* **583**, 253–258 (2020).
30. Sagar, V., Shanahan, L. K., Zelano, C. M., Gottfried, J. A. & Kahnt, T. High-precision mapping reveals the structure of odor coding in the human brain. *Nat. Neurosci.* **26**, 1595–1602 (2023).
31. Schoonover, C. E., Ohashi, S. N., Axel, R. & Fink, A. J. Representational drift in primary olfactory cortex. *Nature* **594**, 541–546 (2021).
32. Gonzalez, J., Torterolo, P., Bolding, K. A. & Tort, A. B. L. Communication subspace dynamics of the canonical olfactory pathway. *iScience* **27**, 12 (2024).
33. Kay, L. M. et al. Olfactory oscillations: the what, how and what for. *Trends Neurosci.* **32**, 207–214 (2009).
34. Rosero, M. A. & Aylwin, M. L. Sniffing shapes the dynamics of olfactory bulb gamma oscillations in awake behaving rats. *Eur. J. Neurosci.* **34**, 787–799 (2011).
35. Stern, M., Bolding, K. A., Abbott, L. & Franks, K. M. A transformation from temporal to ensemble coding in a model of piriform cortex. *eLife* **7**, e34831 (2018).
36. Sagar, V., Shanahan, L. K., Zelano, C. M., Gottfried, J. A. & Kahnt, T. Neural Encoding Models of Olfaction (NEMO) dataset. Zenodo <https://doi.org/10.5281/zenodo.7636722> (2023).
37. Noto, T., Zhou, G., Schuele, S., Templer, J. & Zelano, C. Automated analysis of breathing waveforms using BreathMetrics: a respiratory signal processing toolbox. *Chem. Senses* **43**, 583–597 (2018).
38. Keller, A. & Vosshall, L. B. Olfactory perception of chemically diverse molecules. *BMC Neurosci.* **17**, 1–17 (2016).
39. Keller, A. et al. Predicting human olfactory perception from chemical features of odor molecules. *Science* **355**, 820–826 (2017).
40. Secundo, L. et al. Individual olfactory perception reveals meaningful nonolfactory genetic information. *Proc. Natl Acad. Sci. USA* **112**, 8750–8755 (2015).
41. Bensafi, M., Pouliot, S. & Sobel, N. Odorant-specific patterns of sniffing during imagery distinguish ‘bad’ and ‘good’ olfactory imagers. *Chem. Senses* **30**, 521–529 (2005).
42. Moberly, A. H. et al. Olfactory inputs modulate respiration-related rhythmic activity in the prefrontal cortex and freezing behavior. *Nat. Commun.* **9**, 1528 (2018).
43. Echevarria-Cooper, S. L. et al. Mapping the microstructure and striae of the human olfactory tract with diffusion MRI. *J. Neurosci.* **42**, 58–68 (2021).
44. Zhou, G., Lane, G., Cooper, S. L., Kahnt, T. & Zelano, C. Characterizing functional pathways of the human olfactory system. *eLife* **8**, e47177 (2019).
45. Zelano, C. et al. Nasal respiration entrains human limbic oscillations and modulates cognitive function. *J. Neurosci.* **36**, 12448–12467 (2016).
46. Smear, M., Shusterman, R., O'Connor, R., Bozza, T. & Rinberg, D. Perception of sniff phase in mouse olfaction. *Nature* **479**, 397–400 (2011).
47. Rojas-Líbano, D., Frederick, D. E., Egaña, J. I. & Kay, L. M. The olfactory bulb theta rhythm follows all frequencies of diaphragmatic respiration in the freely behaving rat. *Front. Behav. Neurosci.* **8**, 214 (2014).
48. Fontanini, A. & Bower, J. M. Slow-waves in the olfactory system: an olfactory perspective on cortical rhythms. *Trends Neurosci.* **29**, 429–437 (2006).
49. Adrian, E. The electrical activity of the mammalian olfactory bulb. *Electroencephalogr. Clin. Neurophysiol.* **2**, 377–388 (1950).
50. Liversedge, S. P. & Findlay, J. M. Saccadic eye movements and cognition. *Trends Cogn. Sci.* **4**, 6–14 (2000).
51. Hoffman, J. E. & Subramaniam, B. The role of visual attention in saccadic eye movements. *Percept. Psychophys.* **57**, 787–795 (1995).
52. Ahissar, E. & Arieli, A. Figuring space by time. *Neuron* **32**, 185–201 (2001).
53. Leszczynski, M. & Schroeder, C. E. The role of neuronal oscillations in visual active sensing. *Front. Integr. Neurosci.* **13**, 32 (2019).
54. Rucci, M., Iovin, R., Poletti, M. & Santini, F. Miniature eye movements enhance fine spatial detail. *Nature* **447**, 852–855 (2007).
55. Ko, H.-K., Poletti, M. & Rucci, M. Microsaccades precisely relocate gaze in a high visual acuity task. *Nat. Neurosci.* **13**, 1549–1553 (2010).
56. Szwed, M., Bagdasarian, K. & Ahissar, E. Encoding of vibrissal active touch. *Neuron* **40**, 621–630 (2003).
57. Ganguly, K. & Kleinfeld, D. Goal-directed whisking increases phase-locking between vibrissa movement and electrical activity in primary sensory cortex in rat. *Proc. Natl Acad. Sci. USA* **101**, 12348–12353 (2004).
58. Whitton, J. P., Hancock, K. E. & Polley, D. B. Immersive audiomotor game play enhances neural and perceptual salience of weak signals in noise. *Proc. Natl Acad. Sci. USA* **111**, E2606–E2615 (2014).
59. Kehl, M. S. et al. Single-neuron representations of odours in the human brain. *Nature* **634**, 626–634 (2024).
60. Hernandez, D. E. et al. Fast updating feedback from piriform cortex to the olfactory bulb relays multimodal identity and reward contingency signals during rule-reversal. *Nat. Commun.* **16**, 937 (2025).

61. Cain, W. S. & Murphy, C. L. Interaction between chemoreceptive modalities of odour and irritation. *Nature* **284**, 255–257 (1980).
62. Brand, G. Olfactory/trigeminal interactions in nasal chemoreception. *Neurosci. Biobehav. Rev.* **30**, 908–917 (2006).
63. Frasnelli, J., Charbonneau, G., Collignon, O. & Lepore, F. Odor localization and sniffing. *Chem. Senses* **34**, 139–144 (2009).
64. Rehan, M. et al. Predicting odor pleasantness from odorant structure: pleasantness as a reflection of the physical world. *J. Neurosci.* **27**, 10015–10023 (2007).
65. Zarzo, M. Psychologic dimensions in the perception of everyday odors: pleasantness and edibility. *J. Sens. Stud.* **23**, 354–376 (2008).
66. Yeshurun, Y. & Sobel, N. An odor is not worth a thousand words: from multidimensional odors to unidimensional odor objects. *Ann. Rev. Psychol.* **61**, 219–241 (2010).
67. Noto, T., Zhou, G., Yang, Q., Lane, G. & Zelano, C. Human primary olfactory amygdala subregions form distinct functional networks, suggesting distinct olfactory functions. *Front. Syst. Neurosci.* **15**, 752320 (2021).
68. Scalia, F. & Winans, S. S. The differential projections of the olfactory bulb and accessory olfactory bulb in mammals. *J. Comp. Neurol.* **161**, 31–55 (1975).
69. Carmichael, S. T., Clugnet, M. C. & Price, J. L. Central olfactory connections in the macaque monkey. *J. Comp. Neurol.* **346**, 403–434 (1994).
70. Yang, Q. et al. The human olfactory amygdala: anatomical connections between the olfactory bulb and amygdala subregions. *Imaging Neurosci.* **3**, imag_a_00571 (2025).
71. Sosulski, D. L., Bloom, M. L., Cutforth, T., Axel, R. & Datta, S. R. Distinct representations of olfactory information in different cortical centres. *Nature* **472**, 213–216 (2011).
72. Root, C. M., Denny, C. A., Hen, R. & Axel, R. The participation of cortical amygdala in innate, odour-driven behaviour. *Nature* **515**, 269–273 (2014).
73. Short, S. M. & Wachowiak, M. Temporal dynamics of inhalation-linked activity across defined subpopulations of mouse olfactory bulb neurons imaged in vivo. *eNeuro* **6**, ENEURO.0189-19.2019 (2019).
74. Sobel, N. et al. Odorant-induced and sniff-induced activation in the cerebellum of the human. *J. Neurosci.* **18**, 8990–9001 (1998).
75. Friston, K. J., Williams, S., Howard, R., Frackowiak, R. S. & Turner, R. Movement-related effects in fMRI time-series. *Magn. Reson. Med.* **35**, 346–355 (1996).
76. Prince, J. S. et al. Improving the accuracy of single-trial fMRI response estimates using GLMsingle. *eLife* **11**, e77599 (2022).
77. Allen, E. J. et al. A massive 7T fMRI dataset to bridge cognitive neuroscience and artificial intelligence. *Nat. Neurosci.* **25**, 116–126 (2022).

Acknowledgements

This work was supported by the NIDCD, NIMH and NINDS of the National Institutes of Health under award numbers R01DC015426 (to C.Z.), R01DC018539 (to C.Z.), T32MH067564 (to V.S.) and

T32NS047987 (to V.S.). This research was supported in part by the Intramural Research Program of the National Institutes of Health (NIH) (ZIA DA000642 to T.K.). The contributions of the NIH author (T.K.) are considered works of the United States Government. The findings and conclusions presented in this paper are those of the authors and do not necessarily reflect the views of the NIH or the US Department of Health and Human Services. This research was supported in part through the computational resources and staff contributions provided for the Quest high performance computing facility at Northwestern University, which is jointly supported by the Office of the Provost, the Office for Research and Northwestern University Information Technology. We thank Rockefeller University and Sage Bionetworks-DREAM for the DREAM database of perceptual ratings.

Author contributions

V.S., G.L., T.K. and C.Z. devised the experiment and conceptualized the analyses. A.S., Q.Y. and N.A. collected additional experimental data. V.S., A.S. and G.Z. performed the analyses. V.S., G.L., T.K. and C.Z. prepared and revised the paper.

Competing interests

The authors declare no competing interests.

Additional information

Extended data is available for this paper at <https://doi.org/10.1038/s41562-025-02327-x>.

Supplementary information The online version contains supplementary material available at <https://doi.org/10.1038/s41562-025-02327-x>.

Correspondence and requests for materials should be addressed to Vivek Sagar or Christina Zelano.

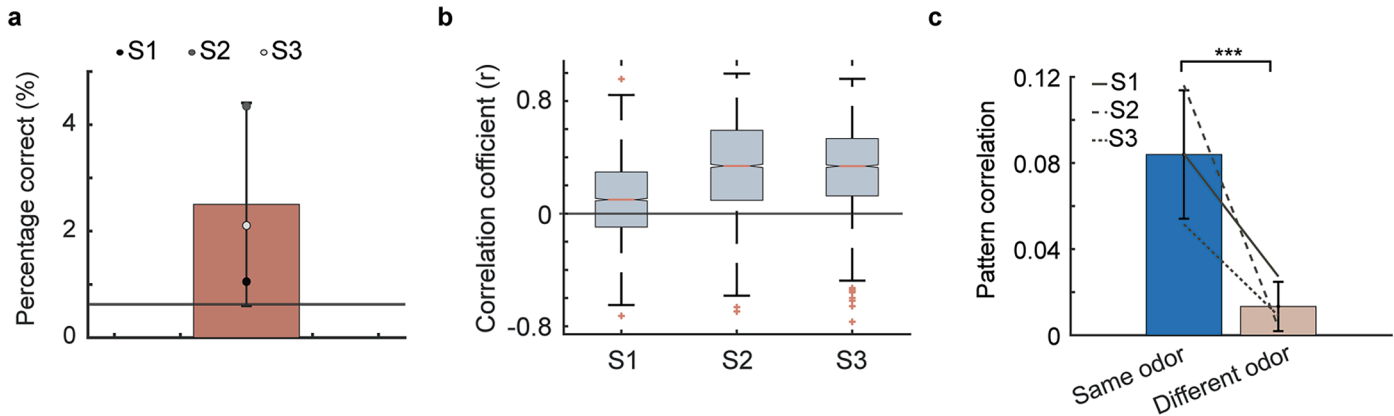
Peer review information *Nature Human Behaviour* thanks Thomas Hummel, Aharon Ravia and the other, anonymous, reviewer(s) for their contribution to the peer review of this work. Peer reviewer reports are available.

Reprints and permissions information is available at www.nature.com/reprints.

Publisher's note Springer Nature remains neutral with regard to jurisdictional claims in published maps and institutional affiliations.

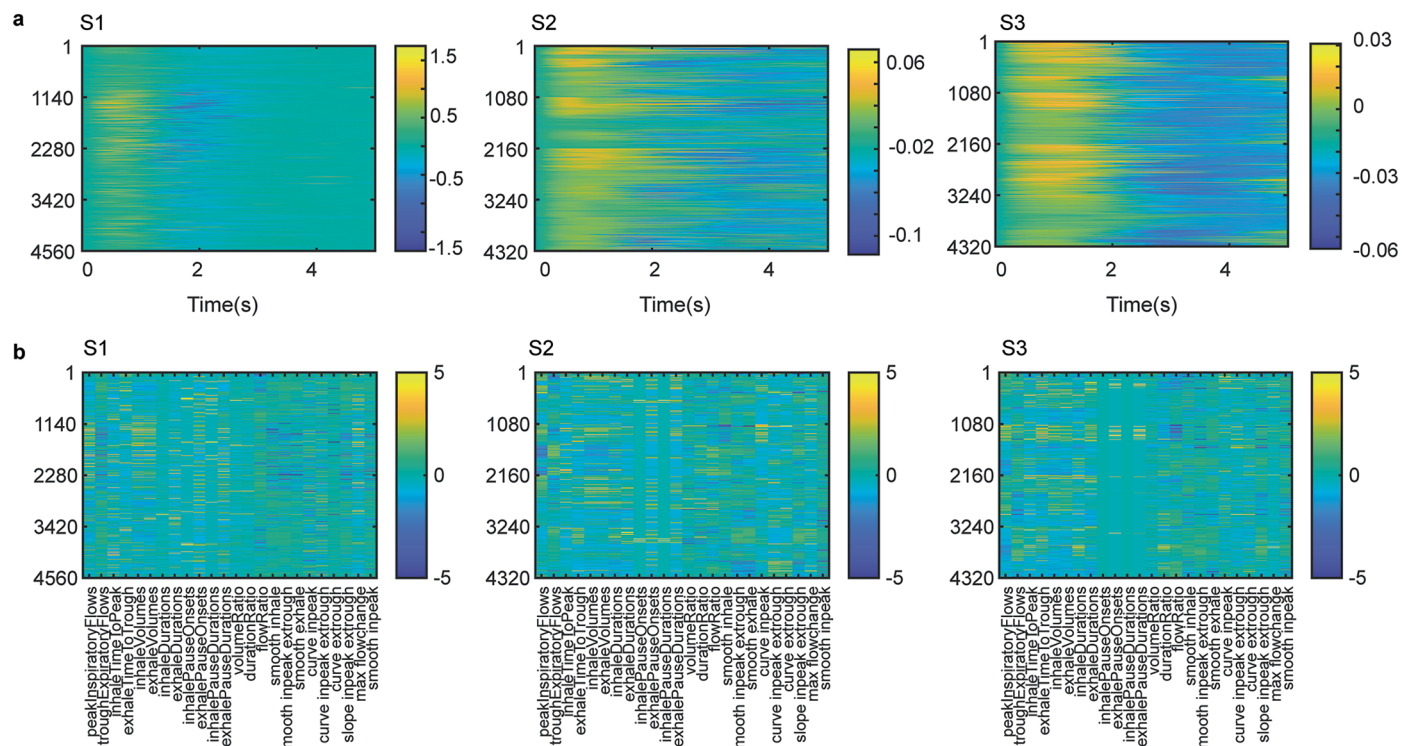
Springer Nature or its licensor (e.g. a society or other partner) holds exclusive rights to this article under a publishing agreement with the author(s) or other rightsholder(s); author self-archiving of the accepted manuscript version of this article is solely governed by the terms of such publishing agreement and applicable law.

© The Author(s), under exclusive licence to Springer Nature Limited 2025

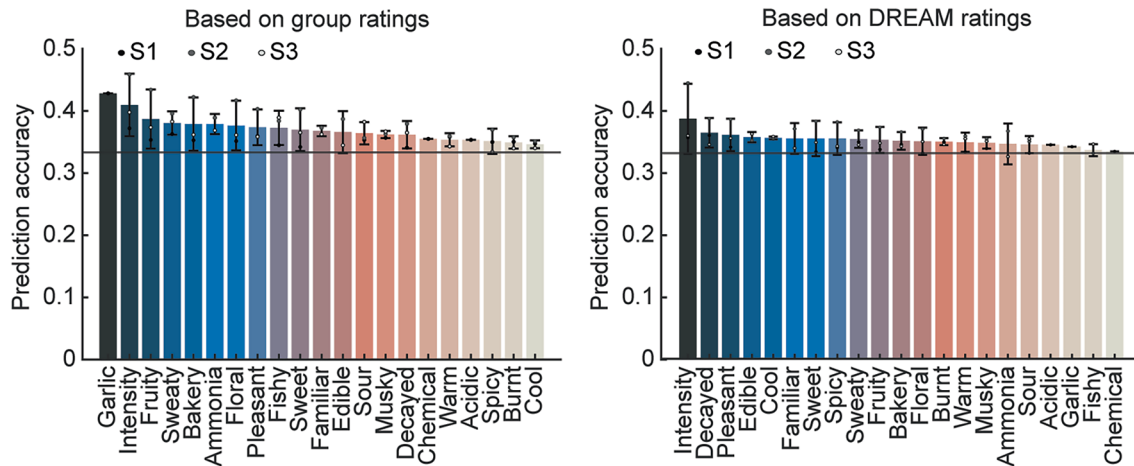


Extended Data Fig. 1 | Decoding accuracy based on raw sniff traces. **a.** Decoding accuracy (percentage of trials reported correctly) of a multiclass SVM model that predicts (out of sample) odor identity based on the raw sniff traces at each trial. Decoding was significant for all subjects (mean subject: classification performance = 2.57%, $P = 0.000$, one-tailed-weighted z-test; all subjects: $P = 0.000$; one-tailed z-test; $N = 4560$ (S1), $N = 4320$ (S2, S3) trials). Data are presented as mean values and error bars indicate 95% C.I. **b.** Distribution of correlation of perceptual ratings (except intensity and pleasantness) between the odor predicted by the classifier in Fig. 2c, and the correct odor, on trials in which the decoder made a wrong prediction. The perceptual ratings of the odor incorrectly predicted by model were significantly correlated to that of correct odor (S1: $r_{\text{SVM}} = 0.097$, $P = 0.000$, 4480 trials, two-tailed Wilcoxon signed rank test; S2: $r_{\text{SVM}} = 0.320$, $P = 0.000$, 4132 trials, two-tailed Wilcoxon signed rank test; S3: r_{SVM}

= 0.309, $P = 0.000$, 4229 trials, two-tailed Wilcoxon signed rank test). Further, this correlation was significant after accounting for mean correlation (r_{mean}) of perceptual ratings among the odors in S2 ($r_{\text{SVM}}r_{\text{mean}} = 0.013$, $P = 0.006$, one-tailed permutation test) and S3 ($r_{\text{SVM}}r_{\text{mean}} = 0.010$, $P = 0.002$, one-tailed permutation test) but not S1 ($r_{\text{SVM}}r_{\text{mean}} = -0.003$, $P = 0.480$, one-tailed permutation test). The center lines denote the median, the box limits denote the upper and lower quartiles, the whiskers are $1.5 \times$ interquartile range and points are outliers. **c.** Pattern correlation analysis after regressing out intensity and pleasantness, showing cross-trial correlation among pairs of trials of the same or different odors ($r_{\text{same}} = 0.083$; $r_{\text{diff}} = 0.013$; for mean subject, $P = 0.000$ for each subject; $N = 4560$ trials in S1 and $N = 4320$ trials in S2 and S3; two-tailed Wilcoxon rank sum test). Data are presented as mean values and error bars indicate 95% C.I.

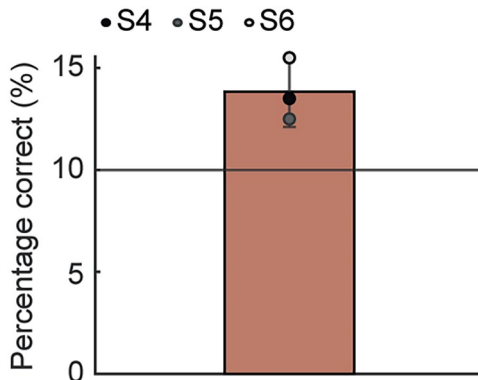


Extended Data Fig. 2 | Subject-wise sniff traces. **a.** Subject-wise sniff traces for all trials used in the study. Trials are sorted in the temporal order of their presentation. **b.** Feature-based representation of sniff trials along 24 features. The first 12 features were extracted from the BreathMetrics toolbox and the remaining were derived features described in the **Methods**.



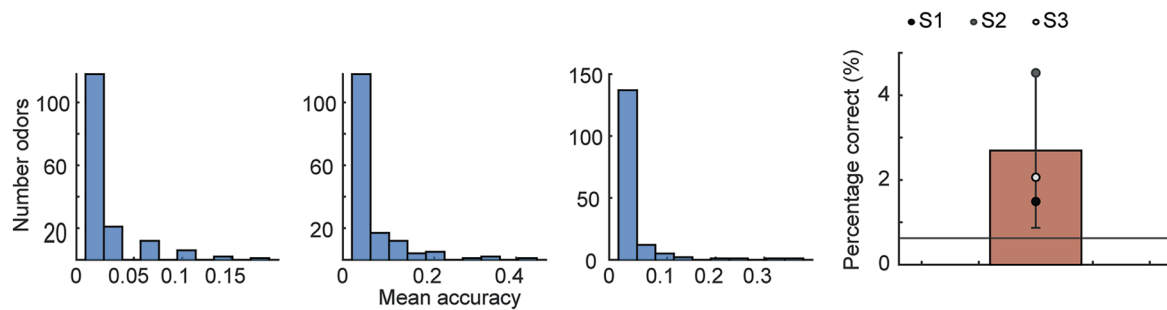
Extended Data Fig. 3 | Multilingual regression models based on group subject data. Performance of multilingual regression models for each descriptor, predicting discretized ratings (low, medium, high) of a perceptual descriptor on a trial, given the sniffing parameters when using average ratings across subjects (left) and ratings from the DREAM dataset (right). Model

performance was significant for several descriptors (chance correct = 33.34%, $P < 0.05$, for 14/21 descriptors in all subjects for group average, and 7/21 descriptors for ratings from the DREAM dataset, one-tailed binomial test (FDR corrected), $N = 4560$ trials in S1 and $N = 4320$ trials in S2 and S3). Data are presented as mean values and error bars indicate 95% C.I.



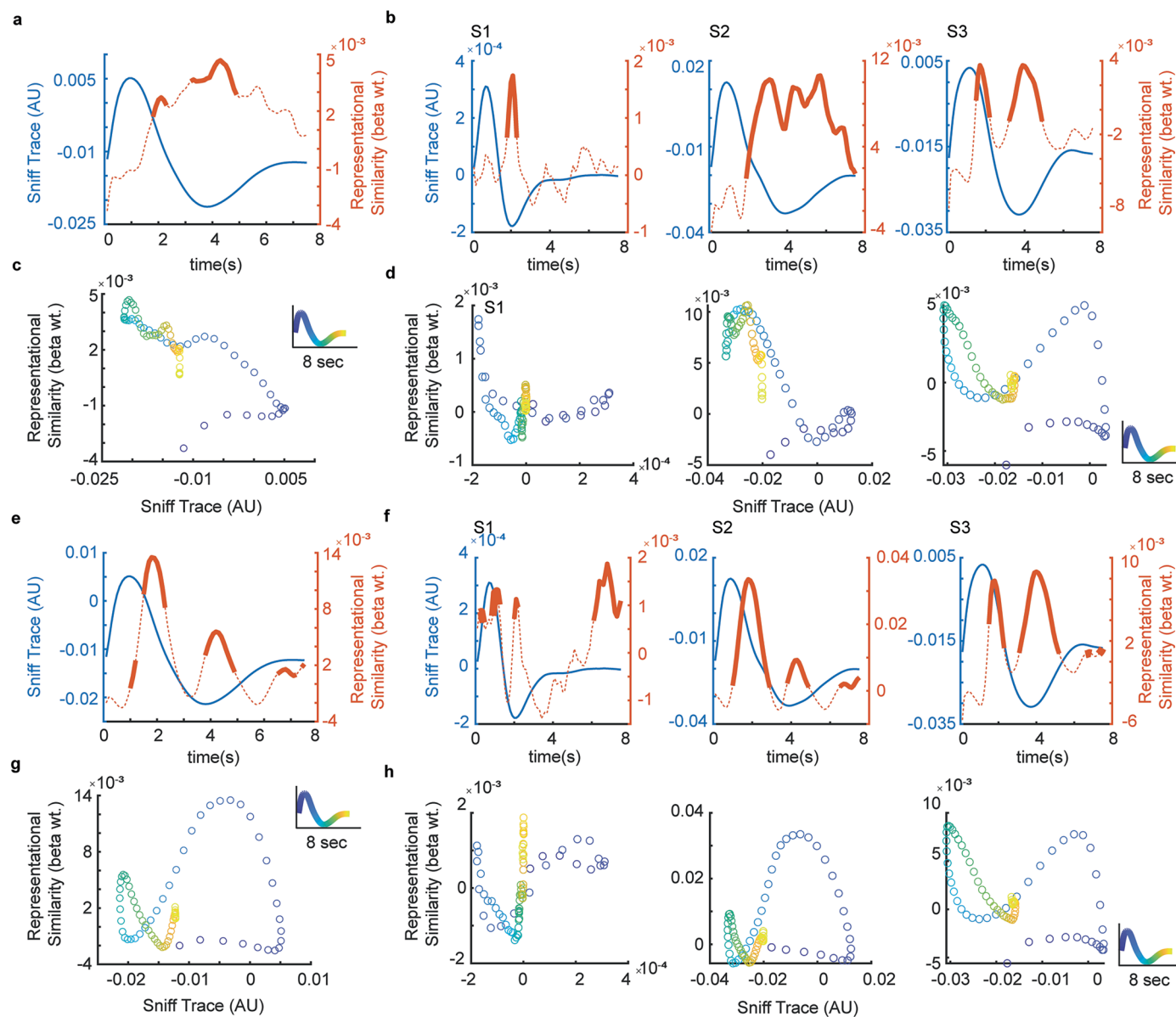
Extended Data Fig. 4 | Odor decoding accuracy from sniffs acquired from additional subjects. Decoding accuracy on additional behavioral data from 3 subjects. Percentage of trials reported correctly of a multiclass SVM model that predicts (out of sample) odor identity for 10 odors based on the features of the

sniff at each trial (200 trials/subject). Together with the 3 original subjects, the combined dataset of 6 subjects shows significant group-level decoding ($P = 0.031, N = 6$, two-tailed Wilcoxon signed rank test), suggesting generalizability of the effect. Data are presented as mean values and error bars indicate 95% C.I.

**Extended Data Fig. 5 | SVM decoding accuracy after accounting for odors with high accuracy.**

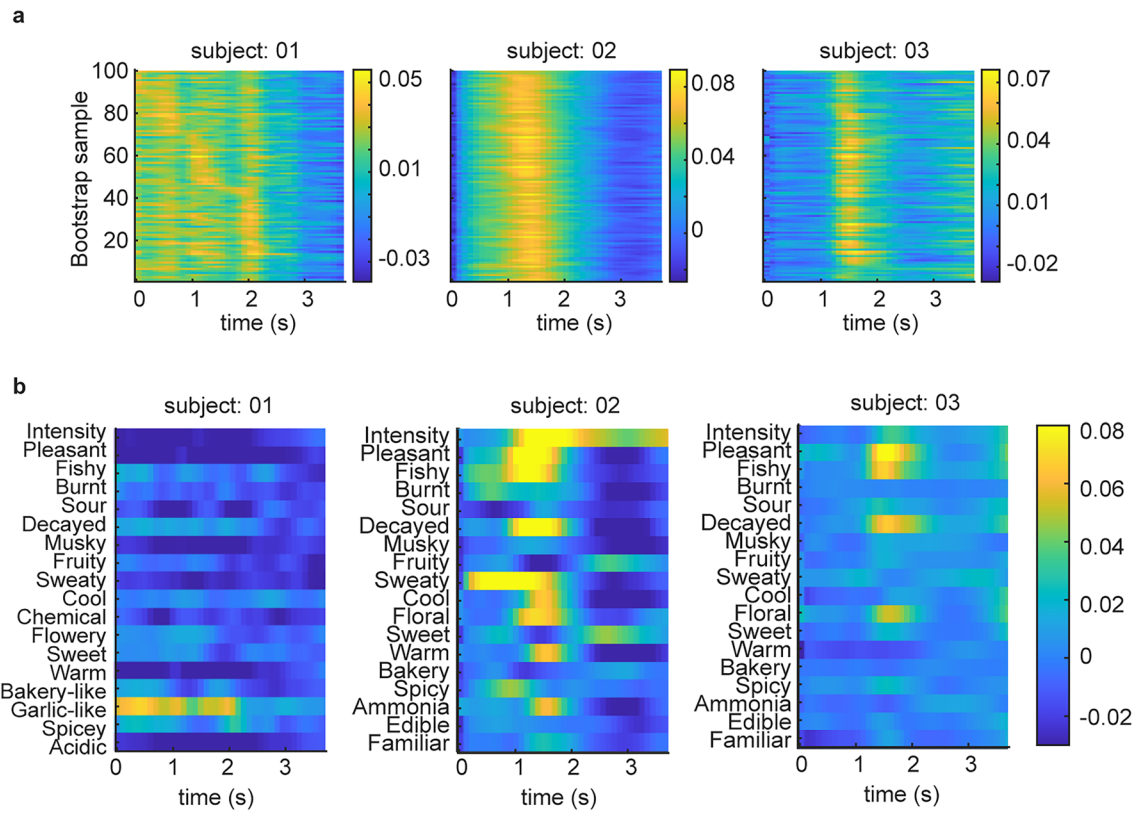
with high accuracy. The left three panels show histograms of mean accuracy (number of trials with significant prediction/total number of trials) per odor for 3 subjects. The right panel shows decoding accuracy (percentage of trials reported correctly) of a multiclass SVM model that predicts (out of sample) odor

identity based on the features of the sniff at each trial, after removing odors that show high prediction accuracy (> 0.2) as seen in the left panels. Decoding was significant for all subjects (mean subject: classification performance = 2.86%, $P = 0.000$, one tailed z-test). Data are presented as mean values and error bars indicate 95% C.I.



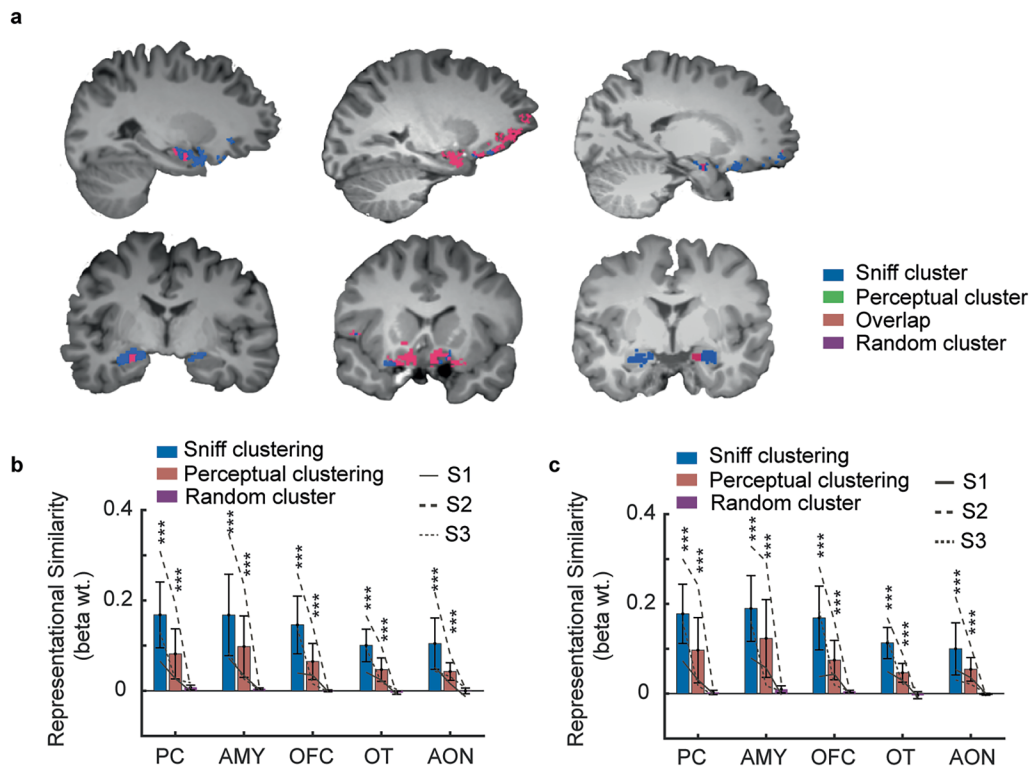
Extended Data Fig. 6 | Subject-wise temporal RSA after accounting for intensity and pleasantness. **a.** The temporal profile of the perceptual similarity regression coefficients (standardized beta values) (orange) overlaid on the sniff flow temporal profile (blue) averaged across subjects when perceptual similarity was based on all descriptors except intensity. Solid lines indicate the time-points when the regression coefficient was significant ($P < 0.05$, subject-wise one-tailed t-test, panel **b** for at least 2/3 subjects) and dashed lines denote otherwise. **b.** Temporal perceptual representational similarity (without intensity) in individual subjects. Solid lines indicate the time-points where the regression coefficient was significant ($P < 0.05$, FDR corrected across time-bins, one-tailed t-test, N = all unique pairs of 4560 (S1), 4320 (S2, S3) trials: 10394520 (S1) and 9329040 (S2, S3)), and dashed lines denote otherwise. **c.** Perceptual representational similarity (without intensity) in **a.** plotted as a function of sniff flow rate. **d.** Perceptual similarity (without intensity) plotted as a function of sniff flow for individual subjects. **e.** The temporal profile of the perceptual

similarity regression coefficients (standardized beta values, orange) overlaid on the sniff flow temporal profile (blue) averaged across subjects when perceptual similarity was based on all descriptors except pleasantness. Solid lines indicate the time-points when the regression coefficient was significant ($P < 0.05$, subject-wise one-tailed t-test, panel **f** for at least 2/3 subjects)) and dashed lines denote otherwise. **f.** Temporal perceptual representational similarity (without pleasantness) for individual subjects. Solid lines indicate the time-points when the regression coefficient was significant ($P < 0.05$, FDR corrected across time-bins, one-tailed t-test, N = all unique pairs of 4560 (S1), 4320 (S2, S3) trials: 10394520 (S1) and 9329040 (S2, S3)) and dashed lines denote otherwise. **g.** Perceptual representational similarity (without pleasantness) in **e.** plotted as a function of sniff flow rate. **h.** Perceptual similarity (without pleasantness) plotted as a function of sniff flow for individual subjects. All subject-wise results were corrected for multiple comparisons across time-bins by an FDR correction (Benjamini-Hochberg procedure).



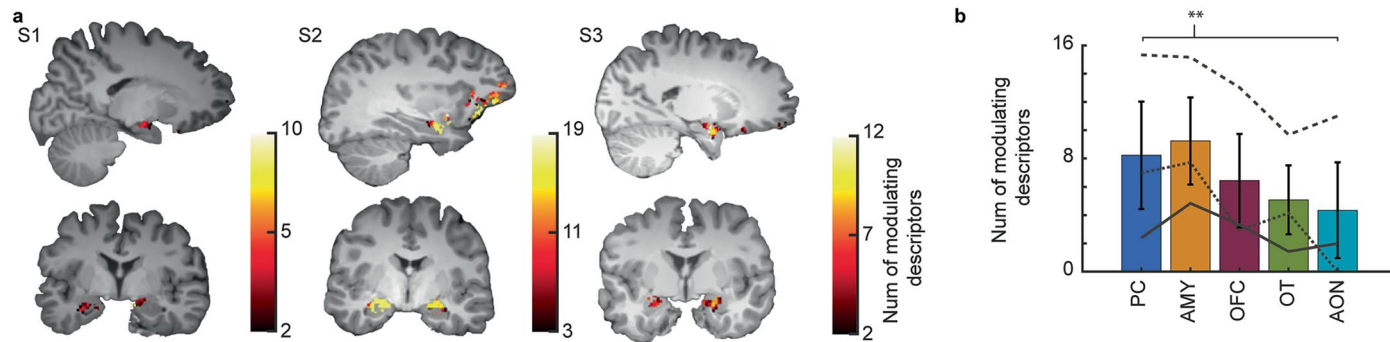
Extended Data Fig. 7 | Temporal RSA for subsets of odors and different perceptual descriptors. **a.** Time series RSA for different subsets of trials, to demonstrate range of variability of information peaks. Rows indicate time-series representational similarities (regression coefficients) for distinct bootstrap

samples while columns indicate separate time-bins. **b.** Time series RSA for different perceptual descriptors. Rows indicate time-series representational similarities (regression coefficients) for distinct descriptors while columns indicate separate time-bins.


Extended Data Fig. 8 | Subject-wise and control analyses for neural RSA.

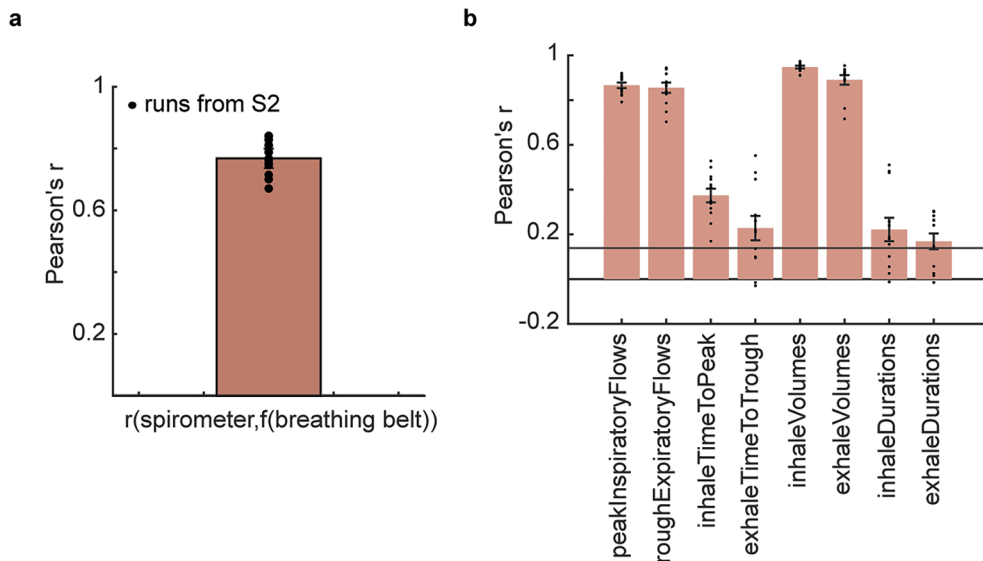
a. Searchlight analyses to determine where representations of sniff shape, perceptual and random clustering of sniffs were significant ($P < 0.05$, t-test, FDR corrected for all conditions and subjects, except S3, perceptual cluster; $P < 0.01$ two-tailed t-test). Raw sniff information (in blue) was pervasive throughout the olfactory regions. A subset of these regions captured aspects of sniff information modulated by perceptual features (red for voxels overlapping with raw sniff voxels, otherwise, green). **b.** Regression coefficients of correlation of sniff-shape/perceptual/random clustered sniff-similarity matrices with correspondingly clustered neural data after orthogonalization of sniff and perceptual clustering. The clustering was orthogonalized using the orthogonalization algorithm described in **Methods** until the adjusted random index (ARI) between the clustering was insignificant (ARI before orthogonalization: S1: 0.003; S2: 0.009; S3: 0.004, $P=0.000$, one-tailed permutation test; ARI after orthogonalization: S1: 0.0004; S2: 0.0008; S3: 0.0005, $P>0.1$, one-tailed permutation test).

Regression coefficients of raw sniffing parameters based on sniff shape were significantly higher than the random control ($P=0.000$, all areas, one-tailed t-test, $N=10394520$ (S1) and 9329040 (S2, S3)). Similarly, regression coefficients of perceptual clustering were significantly higher than the random control ($P=0.000$, all areas, one-tailed t-test, $N=10394520$ (S1) and 9329040 (S2, S3)). **c.** Regression coefficients of correlation of sniff-shape/perceptual/random clustered sniff-similarity matrices with correspondingly clustered neural data based on perceptual features other than intensity and pleasantness. Regression coefficients of raw sniffing parameters based on sniff shape were significantly higher than the random control ($P=0.000$, all areas, one-tailed t-test, $N=10394520$ (S1) and 9329040 (S2, S3)). Similarly, regression coefficients of perceptual clustering were significantly higher than the random control ($P=0.000$, all areas, one-tailed t-test, $N=10394520$ (S1) and 9329040 (S2, S3)). Data are presented as mean values and error bars indicate s.e.m. across subjects in all panels.



Extended Data Fig. 9 | Searchlight-based clustered RSA for individual subjects with control analyses accounting for intensity and pleasantness. **a.** Searchlight-based clustered RSA for individual subjects, with clustering performed on individual perceptual features. The brain maps show number of perceptual features for which the clustered RSA was significant ($P < 0.05$, one-tailed t-test, $N = 10394520$ (S1) and 9329040 (S2, S3)). **b.** Number of perceptual features (except intensity and pleasantness) for which clustered-

RSA was significant across regions (averaged across all odor-responsive voxels at threshold $P = 0.05$, one-tailed t-test). Number of significantly modulating features were highest in the AMY ($F_{4,10132} = 189.788$; $P = 0.000$, repeated measures ANOVA; $P = 0.000$ for post-hoc comparison between AMY and other anatomical regions, except PC; $P = 0.009$, pairwise t-test, FDR corrected). Data are presented as mean values and error bars indicate s.e.m. across subjects in all panels.



Extended Data Fig. 10 | Similarity between measuring sniffs from breathing belt and spirometer. **a.** Pearson's r of raw sniff trace obtained from spirometer and derivative of breathing belt for 12 runs. Correlation is across a large number of samples ($>10^6$) and is highly significant ($P=0.000$, mean $r=0.768$, $N=1209200$ samples for the shortest run, two-tailed t-test) **b.** Pearson's r of sniff features extracted from the BreathMetrics toolbox for spirometer trace and

derivative of breathing belt for all runs. Chance r is shown in black line and the correlation is significant in all features (all $P<0.001$, one-tailed t-test, except exhaleTimeToTrough: $P=0.0006$; inhaleDurations: $P=0.004$ and exhaleDurations: $P=0.027$, $N=141$ (mean number of sniffs in each run)). For all panels data are presented as mean values and error bars indicate s.e.m. across runs.

Reporting Summary

Nature Portfolio wishes to improve the reproducibility of the work that we publish. This form provides structure for consistency and transparency in reporting. For further information on Nature Portfolio policies, see our [Editorial Policies](#) and the [Editorial Policy Checklist](#).

Statistics

For all statistical analyses, confirm that the following items are present in the figure legend, table legend, main text, or Methods section.

n/a Confirmed

- The exact sample size (n) for each experimental group/condition, given as a discrete number and unit of measurement
- A statement on whether measurements were taken from distinct samples or whether the same sample was measured repeatedly
- The statistical test(s) used AND whether they are one- or two-sided
Only common tests should be described solely by name; describe more complex techniques in the Methods section.
- A description of all covariates tested
- A description of any assumptions or corrections, such as tests of normality and adjustment for multiple comparisons
- A full description of the statistical parameters including central tendency (e.g. means) or other basic estimates (e.g. regression coefficient) AND variation (e.g. standard deviation) or associated estimates of uncertainty (e.g. confidence intervals)
- For null hypothesis testing, the test statistic (e.g. F , t , r) with confidence intervals, effect sizes, degrees of freedom and P value noted
Give P values as exact values whenever suitable.
- For Bayesian analysis, information on the choice of priors and Markov chain Monte Carlo settings
- For hierarchical and complex designs, identification of the appropriate level for tests and full reporting of outcomes
- Estimates of effect sizes (e.g. Cohen's d , Pearson's r), indicating how they were calculated

Our web collection on [statistics for biologists](#) contains articles on many of the points above.

Software and code

Policy information about [availability of computer code](#)

Data collection	Custom Code, COGENT 2000, MATLAB R2016b;
Data analysis	Custom code(Link https://github.com/viveksgsr/SFP), BreathMetrics, LibSVM, SPM 12, GLMsingle Package, MATLAB R2020b, MATLAB R2023b

For manuscripts utilizing custom algorithms or software that are central to the research but not yet described in published literature, software must be made available to editors and reviewers. We strongly encourage code deposition in a community repository (e.g. GitHub). See the Nature Portfolio [guidelines for submitting code & software](#) for further information.

Data

Policy information about [availability of data](#)

All manuscripts must include a [data availability statement](#). This statement should provide the following information, where applicable:

- Accession codes, unique identifiers, or web links for publicly available datasets
- A description of any restrictions on data availability
- For clinical datasets or third party data, please ensure that the statement adheres to our [policy](#)

Analyses presented in this manuscript are based on previously published database. Additional behavioral data for group level analyses is available on <https://github.com/viveksgsr/SFP>.

<https://www.nature.com/articles/s41593-023-01414-4>
<https://zenodo.org/records/7636722>

Research involving human participants, their data, or biological material

Policy information about studies with [human participants or human data](#). See also policy information about [sex, gender \(identity/presentation\), and sexual orientation](#) and [race, ethnicity and racism](#).

Reporting on sex and gender

The study involved 3 human subjects (2 Female, 1 Male). Additional followup behavioral experiment involved 3 additional subjects (2 Female, 1 Male). Participants were asked to self-identify their biological sex with an option to not report it. The demographic survey was based on NIH guidelines and approved by IRB. We did not collect gender information since we did not consider that gender was likely to influence our main findings. We did not perform analyses that compared influence of sex on our findings since the primary focus of this experiment was to probe the effects of odor information on sniff modulation in an individual which was likely to be unaffected by gender or sex.

Reporting on race, ethnicity, or other socially relevant groupings

Subjects were asked to report their race and ethnicity (or prefer not to answer). The demographic survey was based on NIH guidelines and approved by IRB. We did not consider race or ethnicity as a proxy for socioeconomic status. We did not perform any analyses that compared influence of race or ethnicity on our findings since the primary focus of this experiment was to probe the effects of odor information on sniff modulation in an individual which was likely to be unaffected by race or ethnicity.

Population characteristics

Sample consisted of three healthy human subjects (2 females ages 23-24, 1 male age 24) for the primary analyses. Additional behavioral followup analysis involved 3 additional subjects (2 female ages 28-30, 1 male age 44). Subjects were right-handed, native English speakers with normal or corrected to normal vision. Subjects had no history of prior psychiatric or neurological disorders, no significant medical disorders, no smell and taste dysfunction or a history of sinusitis or allergic rhinitis and were not using medications that could affect alertness.

Recruitment

The first set of subjects were recruited through the Kahnt Lab Research Registry. Second set of subjects for follow up analyses were recruited through the Zelano lab database.

Ethics oversight

Institute Review Board at Northwestern University approved the original dataset and the subsequent analyses

Note that full information on the approval of the study protocol must also be provided in the manuscript.

Field-specific reporting

Please select the one below that is the best fit for your research. If you are not sure, read the appropriate sections before making your selection.

Life sciences Behavioural & social sciences Ecological, evolutionary & environmental sciences

For a reference copy of the document with all sections, see nature.com/documents/nr-reporting-summary-flat.pdf

Life sciences study design

All studies must disclose on these points even when the disclosure is negative.

Sample size	160 odor stimuli (conditions, 27-30 repetitions each) were tested in 3 independent subjects. No sample size estimation was done. We chose a precision approach involving many stimuli and repetitions in a small number of subjects, and statistics were computed within subjects.
Data exclusions	No data was excluded from the previously published dataset. Original dataset removed one additional subject due to a psychiatric disorder that was disclosed later.
Replication	Each of the 160 odor stimuli were repeated 27-30 times in each of the three subjects.
Randomization	In this study with a within-subject design, the order the stimuli was randomized across experimental sessions.
Blinding	Single-blind. Subjects were blinded with respect to the order of the conditions.

Reporting for specific materials, systems and methods

We require information from authors about some types of materials, experimental systems and methods used in many studies. Here, indicate whether each material, system or method listed is relevant to your study. If you are not sure if a list item applies to your research, read the appropriate section before selecting a response.

Materials & experimental systems

n/a	Involved in the study
<input checked="" type="checkbox"/>	Antibodies
<input checked="" type="checkbox"/>	Eukaryotic cell lines
<input checked="" type="checkbox"/>	Palaeontology and archaeology
<input checked="" type="checkbox"/>	Animals and other organisms
<input checked="" type="checkbox"/>	Clinical data
<input checked="" type="checkbox"/>	Dual use research of concern
<input checked="" type="checkbox"/>	Plants

Methods

n/a	Involved in the study
<input checked="" type="checkbox"/>	ChIP-seq
<input checked="" type="checkbox"/>	Flow cytometry
<input type="checkbox"/>	MRI-based neuroimaging

Plants

Seed stocks

N/A

Novel plant genotypes

N/A

Authentication

N/A

Magnetic resonance imaging

Experimental design

Design type

Task-based event-related design.

Design specifications

Each subject was presented with 160 odor stimuli, each repeated 27-30 times. There were 12 fMRI sessions per subject, each up to 2 hours in duration and consisted of 4 runs. Each run consisted of 10 odor stimuli presented across 90-100 trials. Each odor stimulus was presented in 3 sessions resulting in 27-30 trials per stimulus per subject.

Behavioral performance measures

In each trial, subjects responded if they could smell the odor stimulus. If they could, they rated the odor on one perceptual descriptor. Their rating, button press and reaction times were recorded. Consistency of perceptual ratings over repeated presentations of the odor stimuli was quantified using Pearson's correlation.

Acquisition

Imaging type(s)

Functional and Structural

Field strength

3T

Sequence & imaging parameters

Gradient echo T2* weighted echoplanar images were acquired during the functional scan. For subject 1: repetition time (TR) = 1.4 seconds, echo time (TE) = 22ms, matrix size = 104x96 voxels, flip angle = 80°, in-plane resolution = 2x2mm, slice thickness = 2mm, multiband factor (MB) = 2, 42 slices. To further optimize the spatial coverage in subjects 2 and 3, small adjustment to the scanning sequence were made (TE = 24ms, flip angle = 70°, matrix size = 122x102 voxels, in-plane resolution = 1.7x1.7mm, slice thickness = 2mm, MB = 3, 38 slices). High-resolution T1 weighed anatomical images (1mm³ isotropic) were acquired for anatomical localization with the following parameters: TR = 2170 ms; TE = 1.69 ms; flip angle, 7°, 1 mm isotropic voxels, no gap, number of slices = 256; field of view= 176 mm x 256 mm x 256 mm).

Area of acquisition

The imaging sequence was optimized for signal recovery in olfactory areas. Functional images were acquired at an acquisition angle= 30° rostral to the inter-commissural line, slices per image = 42 in subject 1 and slices per image = 38 in subject 2 and 3.

Diffusion MRI

 Used Not used

Preprocessing

Preprocessing software

Default functions in SPM12 were used to realign the functional images and coregister them to the anatomical image. Functional images were smoothed using a 2mm³ FWHM gaussian kernel. The anatomical image was segmented to extract gray matter voxels. GLMsingle package was used to extract single trial responses for each voxel.

Normalization

Data was analyzed in the native space without normalization. However final brain maps exhibiting sniff modulations was

Normalization	normalized using SPM's default settings (with very light regularization (0.0001), bias FWHM of 60mm cutoff, tissue probability map (TPM) from SPM and MNI space for affine regularization)
Normalization template	Data was normalized using MNI template
Noise and artifact removal	Translation and rotation parameters estimated during the realignment procedure were used as nuisance regressors to account for motion-related effects. Additional nuisance regressors were appended to account for the difference and variance in interleaved sets of slices within volumes.
Volume censoring	Volumes for which slice difference and variability exceeded 5 units of signal to noise ratio (mean/standard deviation) were effectively excluded by including additional regressors for slice difference and variability in the general linear model.

Statistical modeling & inference

Model type and settings	Representational Similarity Analysis (RSA)
Effect(s) tested	Pearson's correlation of neural similarity in an ROI with similarity in sniffs (grouped either based on sniff shape or odor percept)
Specify type of analysis:	<input type="checkbox"/> Whole brain <input checked="" type="checkbox"/> ROI-based <input type="checkbox"/> Both
Anatomical location(s)	Analysis was restricted to major olfactory areas: piriform cortices, amygdala, orbitofrontal cortex, olfactory tubercle and anterior olfactory nucleus. These ROIs were drawn in MNI space and inverse-normalized to subjects' native space.
Statistic type for inference	ROI-wise and searchlight based analyses

(See [Eklund et al. 2016](#))

Correction	Brain maps for representational similarity analysis were corrected for multiple comparisons using FDR correction.
Models & analysis	

n/a	Involved in the study
<input checked="" type="checkbox"/>	<input type="checkbox"/> Functional and/or effective connectivity
<input checked="" type="checkbox"/>	<input type="checkbox"/> Graph analysis
<input type="checkbox"/>	<input checked="" type="checkbox"/> Multivariate modeling or predictive analysis
Multivariate modeling and predictive analysis	Searchlight and ROI based approach was used to relate the similarity of neural data with similarity in sniffs (grouped based on shapes or odor information)